A detailed description of the computer implementation of SHCC material model in OOFEM.

Czech Technical University in Prague
Faculty of Civil Engineering
Department of Mechanics
Thákurova 7
166 29 Prague 6

Petr Havlásek petr.havlasek@fsv.cvut.cz
Petr Kabele petr.kabele@fsv.cvut.cz

February 1, 2017

Contents

1 Notation

CAF ... continuous aligned fibers
SAF ... short aligned fibers
SRF ... short random fibers
COD ... crack opening displacement [m]
CSD ... crack slipping displacement [m]
a ... length of the fiber debonded length [m]
a_g ... aggregate size [m]
c_1, c_2 ... constants in Hordijk's law [-]
b_0–b_3 ... parameters of bond shear strength [-]
f ... snubbing coefficient [-]
g ... snubbing factor [-]
f_c ... matrix compressive strength [-]
f_t ... matrix tensile strength [-]
k ... fiber cross-section shape correction factor [-]
s_F ... shear factor coefficient [-]
u, u_i ... crack shear slip (ditto for i-th crack) [m]
$\hat{u}$ ... crack shear slip adjusted by N_{cr} [m]
w, w_i ... crack opening (ditto for i-th crack) [m]
w_{max} ... maximum crack opening [m]
w_f ... characteristic crack opening (for lin. model failure) [m]
Δw ... activation opening [m]
$\bar{w}$ ... stress-dependent crack opening $= w - \Delta w$
w^* ... transitional crack opening [m]
$\hat{w}$ ... crack opening adjusted by N_{cr} [m]
x ... distance from the crack [m]
D ... stiffness matrix
D_e ... elastic stiffness matrix
$D_{cr,T}$ ... local tangent stiffness matrix of crack
$D_{cr,S}$ ... local secant stiffness matrix of crack
D_f ... fiber diameter [m]
$D_{I,T}$ ... tangent stiffness in mode I (opening) [Pa]
$D_{I,S}$ ... secant stiffness in mode I (opening) [Pa]
D_{II} ... stiffness in mode II (shearing) [Pa]
$D_{*,f}$ ... crack stiffness due to fibers only [Pa]
$D_{*,m}$ ... crack stiffness due to matrix only [Pa]
$D_{*,\omega}$ ... damage-influenced crack stiffness [Pa]

$\hat{D}_*$ ... crack stiffness effected by the number of parallel cracks [Pa]
E_m ... Young's modulus of matrix [Pa]
E_f ... Young's modulus of fibers [Pa]
F_a ... fiber anchoring force [N]
F_0 ... resultant of shear stress on fiber surface [N]
G_m ... shear modulus of matrix [Pa]
G_f ... shear modulus of fibers [Pa]
G_f ... fracture energy [N/m]
G_c ... shear stiffness of a cracked composite [Pa]
H ... linear hardening modulus [Pa]
L ... element size (projection) [m]
$\hat{L}$ ... element size adjusted by N_{cr} [m]
L_f ... fiber length [m]
M ... exponent in the softening law [-]
N_{cr} ... number of parallel cracks in element [-]
V_m ... matrix volume ratio [-]
V_f ... fiber volume ratio [-]
$\bar{V}_f$ ... effective fiber volume ratio [-]
V_f^{ast} ... damage-affected fiber volume ratio [-]
β ... shear retention factor [-]
β_f ... shear retention factor due to fibers only [-]
β_m ... shear retention factor due to matrix only [-]
γ ... shear strain [-]
γ_{el} ... shear elastic strain [-]
γ_{cr} ... shear cracking strain [-]
γ_f ... crack shear deformation [-]
γ_{fc} ... damage parameter (crack shear deformation) [-]
ε ... normal strain [-]
ε_{el} ... normal elastic strain [-]
ε_{cr} ... normal cracking strain [-]
ε_m ... elastic strain if matrix [-]
ε_f ... elastic strain of fibers [-]
Δ ... fiber pull-out displacement [-]
η ... auxiliary constant depending on E_f, E_m and V_f [-]
λ ... auxiliary constant for SRF [-]
σ ... normal stress [Pa]
σ_b ... (total) bridging stress [Pa]
$\sigma_{b,f}$ ... bridging stress in fibers (nominal, per unit area of crack) [Pa]

σ_f ... nominal stress in fibers (per unit area) [Pa]
$\bar{\sigma}_f$ ... effective stress in fibers (per area of fibers) [Pa]
$\sigma_{b,m}$ ... bridging stress in matrix (nominal, per unit area of crack) [Pa]
σ_m ... nominal stress in matrix (per unit area) [Pa]
$\bar{\sigma}_{b,m}$ ... bridging stress in matrix (effective, per area of matrix) [Pa]
$\bar{\sigma}_m$ ... effective stress in matrix (per area of matrix) [Pa]
τ ... shear stress [Pa]
τ ... frictional shear stress between fiber and matrix during fiber pullout [Pa]
τ_0 ... frictional shear stress between fiber and matrix during debonding [Pa]
τ_b ... bridging shear stress in (per unit area) [Pa]
$\tau_{b,f}$ ... bridging shear stress in fibers (nominal, per unit area of crack) [Pa]
$\tau_{b,m}$ ... bridging shear stress in matrix (nominal, per unit area of crack) [Pa]
θ ... angle between crack plane normal and fiber [-]
ω ... scalar damage [-]

2 Introduction and General Information

This manual summarizes the main methods and algorithms developed in order to realistically simulate the short-time mechanical behavior of fiber-reinforced cementitious composites with strain hardening. These methods have been implemented in the open-source finite element package OOFEM [9], [10], [11]. This manual provides also examples of material definition syntax used in OOFEM.

The main features and assets of the new implementation are (among others):

- cohesive crack model with fixed (not rotating) orientation of crack planes
- cohesive laws capturing the behavior of both plain and fiber reinforced composites
- the most common as well as user-defined traction-separation laws of matrix
- traction-separation laws for fibers depending almost entirely on the physical properties, quantity, alignment (orientation) and type
- evolving degradation of shear stiffness after cracking
- crack shearing leading to fiber damage
- crack-spacing concept (multiple parallel cracks) for large elements
- nonlocal model guaranteeing objective results for strain hardening materials and fine finite element mesh

Interesting quantities computed by the program can be parsered and extracted by a python program *python.py* (available at OOFEM.org) and then displayed using e.g. Gnuplot (free & open-source) [12] or your favorite spreadsheet program. The results can be also exported into a set of **.vtu* files and then visualized in Paraview (free & open-source) [2]. The current version of the source files can be obtained at the OOFEM git repository http://oofem.org/gitweb/ and then compiled. The next release (version 2.5) containing the new material model is expected in the mid-2017. The executable version of OOFEM for Windows 32-bit (which can be used not only to run the tests and benchmarks of the new model) is availabe at the web page where you found this documentation.

The models presented hereafter are suitable for representation of individual cracks in plain as well as fiber reinforced cementitious composites. It can be used to simulate localized cracks in composites, which exhibit tension softening

behavior, such as fiber reinforced concrete (FRC), high strength FRC (HSFRC) or softening or mildly hardening type of ultra high-performance FRC (UHPFRC). The model, however, is also applicable for tension hardening composites, which exhibit multiple cracking behavior, such as engineered cementitious composites (ECC) or strain hardening fiber reinforced cementitious composites (SHCC).

Post-cracking tensile and shear response is modeled using the concept of a cohesive crack. In this approach, a crack is perceived as a displacement discontinuity, which is capable of transferring traction between its faces. The normal traction is related to the crack opening displacement through traction-separation law. The resulting composite traction-separation relationship on crack is considered as the combination of matrix bridging and fiber bridging. The fiber bridging model is based on micromechanics of fiber debonding and pullout. Crack sliding is allowed by the reduction of the shear stiffness at the cracked material point.

The implementation exploits the object-oriented structure of OOFEM. The parent abstract class *Fixed crack model* `FCM` provides only the general structure for the stiffness matrices and the stress-return algorithm; this class is derived from the `Structural Material class`. The constitutive laws for crack opening and shearing of plain concrete are implemented in `ConcreteFCM` class. This model is a parent of the *Fixed crack model for FRC*, `FRCFCM`, which introduces material laws for different kinds of fibers and the overall stress/stiffness is evaluated according to the volume fraction of matrix and fibers. Simulations of strain hardening cementitious materials on a fine finite element mesh can give objective results only when using *Nonlocal fixed crack model for SHCC* defined in `NLFRCFCM` class.

The theory behind the new model is based on [1], [7], [5], [6], [13], [4], [8], [14], [3].

3 Fixed crack model - overview

This section describes the implementation of the fixed crack model. Before the onset of cracking, the material is modeled as isotropic linear elastic characterized by Young's modulus and Poisson's ratio. Cracking is initiated when principal stress reaches tensile strength. Further loading is governed by a softening law. Proper amount energy dissipation is guaranteed by the crack-band approach, the width of the crack band is given by the size of the finite element projected in the direction of the principal stress. Multiple cracking is allowed, the maximum number of cracks is controlled by *ncracks* parameter. Only mutually perpendicular cracks are supported. If cracking occurs in more directions, the behavior on the crack planes is considered to be independent. The secant stiffness is used for unloading and reloading. In compression regime, this model corresponds to an isotropic linear elastic material.

Once the the strength of the material has been reached, further loading is the normal direction to the crack plane is governed by one of the traction-separation or traction-crack strain laws. In the direction normal to the crack plane, the total normal strain ε is subdivided into the elastic strain ε_{el} and cracking strain ε_{cr}. In a similar fashion, the total shear strain γ is subdivided into the elastic γ_{el} and cracking shear strain γ_{cr}. Correct split of the total deformation into the elastic and cracking component is implemented in the `GiveRealStresVector` method, the algorithm uses initially gradient method and subsequently bisection should the gradient method fail.

3.1 Stiffness matrices and stresses

The elastic stiffness matrix D_e is constructed from the effective Young's modulus and Poisson's ratio. The effective Young's modulus of material without fibers is equal to the conventional Young's modulus.

The secant and tangent stiffness matrices in the local coordinate system (given by the crack directions) are computed as

$$D = D_e - D_e \left(D_e + D_{cr,S}\right)^{-1} D_e \tag{1}$$

$$D = D_e - D_e \left(D_e + D_{cr,T}\right)^{-1} D_e \tag{2}$$

where $D_{cr,S}/D_{cr,T}$ is the local tangent/secant stiffness matrix of the cohesive crack(s) and is diagonal. First three components of $D_{cr,S}$ are associated with the normal crack directions and are computed as $\sigma_i(u_{i,max}, w_{i,max})/\varepsilon_{cr,i}$ while in

the tangent stiffness matrix $D_{cr,T}$ as $\partial\sigma_i(u_i, w_i)/\partial\varepsilon_{cr,i}$. In both cases the shear components (4th-6th) are the same, $D_{II}(u_i, w_i)$.

A global stiffness matrix is obtained by rotating the local stiffness matrix by the transformation matrix for strain. The shear components in the local stiffness matrix D are equal to G_c which is introduced in the next section.

Stresses in the local coordinate system are computed as

$$\sigma = D_{cr,S}\varepsilon_{cr} \tag{3}$$

3.2 Shear and shear stiffness of a cracked element

There are two stiffnesses associated with shear which need to be distinguished. The first one is the effective shear stiffness of a cracked composite G_c which is needed when constructing the stiffness matrix; the second one is the crack stiffness in shearing mode, D_{II} which is necessary in finding the equilibrium at the material point level (split of total strain into cracking strain and elastic strain).

Both stiffnesses can be used to calculate the shear stress. The first option is

$$\tau = G_c\gamma \tag{4}$$

where γ is the total strain. The second option is

$$\tau = D_{II,S}\gamma_{cr} \tag{5}$$

where γ_{cr} is the cracking part of the shear strain.

The calculated shear stress can be cropped by τ_{max} which is the crack shear strength and depends on the crack opening and crack shear slip.

Current implementation of the fixed crack model supports several different ways to reflect the decrease in shear stiffness triggered by crack initiation. One option is the shear retention factor, β which relates the stiffnesses of the cracked and uncracked material

$$G_c = \beta G \tag{6}$$

Another option is the shear factor coefficient s_F which links the stiffness in mode II to mode I

$$D_{II} = s_F D_{I,S} \tag{7}$$

Naturally, using the following equation, the crack shear stiffness can be converted into the shear retention factor and vice versa

$$\frac{1}{G_c} = \frac{1}{\beta G} = \frac{1}{G} + \frac{1}{D_{II}} \tag{8}$$

$$\beta = \frac{D_{II}}{D_{II} + G} \tag{9}$$

$$D_{II} = \frac{\beta G}{1 - \beta} \tag{10}$$

3.3 Extension to multiple cracks

The formulae from the previous section can be easily generalized to case with multiple perpendicular cracks. In terms of the shear strain the only difference is that the cracking strain is now split into two components, $\gamma_{cr,1}$ (first crack) and $\gamma_{cr,2}$ (second crack).

$$\gamma = \gamma_{el} + \gamma_{cr} = \gamma_{el} + \gamma_{cr,1} + \gamma_{cr,2} \tag{11}$$

Naturally, any additional crack leads to an increase in shear compliance. Total shear stiffness is given by the stiffness of three serially coupled units. The reciprocal value of the effective shear modulus thus becomes

$$\frac{1}{G_c} = \frac{1}{\beta G} = \frac{1}{G} + \frac{1}{D_{II,1}(w_1)} + \frac{1}{D_{II,2}(w_2)} \tag{12}$$

where the first fraction on the right hand side of the equation is linked to the elastic shear deformation γ_{el} and the subsequent two terms to $\gamma_{cr,1}$ and $\gamma_{cr,2}$.

The effective shear retention factor expressed in terms of the crack stiffnesses in shear is evaluated as

$$\beta = \frac{1}{1 + G\left(\frac{1}{D_{II,1}} + \frac{1}{D_{II,2}}\right)} \tag{13}$$

The optional keyword *multipleCrackShear* defines how to calculate the effective shear stiffness G_c and crack shear stiffness D_{II}. If this keyword is not provided, the shear stiffness is determined from the dominant crack only, in the other case it is computed using equations (12) and (18).

3.4 Crack opening and crack slip

Employing the crack-band approach, the crack opening (in the local coordinate system) is obtained from the normal cracking strain

$$w_i = L_i \varepsilon_{cr,i} \tag{14}$$

where L_i is the element size (projected normal to the i-th crack plane).

Crack sliding is computed in a similar fashion. Although, the problem can become more complex because in general more than one crack can contribute to the same shear cracking strain.

In the case of one crack the situation is very simple, crack slip is computed as

$$u = L\gamma_{cr} \tag{15}$$

where u is the crack slip (in direction of the crack plane) and L is the element length (projection of the finite element in direction perpendicular to the crack plane normal vector).

If more than one crack develops at one integration point in 2D, the shear stress τ remains equal to both bridging shear stresses $\tau_{b,i}$ and $\tau_{b,j}$. Total shear cracking strain can be split into the individual cracks as

$$\gamma_{cr} = \gamma_{cr,i} + \gamma_{cr,j} \tag{16}$$

which can be written as

$$\frac{\tau}{D_{II}} = \frac{\tau}{D_{II,i}} + \frac{\tau}{D_{II,j}} \tag{17}$$

The total total cracking shear stiffness can be evaluated from the last equation as

$$D_{II} = \frac{D_{II,i} D_{II,j}}{D_{II,i} + D_{II,j}} \tag{18}$$

The total cracking shear deformation is then distributed to the cracks according to their stiffnesses.

$$\frac{\gamma_{cr,i}}{\gamma_{cr}} = \frac{1/D_{II,i}}{1/D_{II}} = \frac{D_{II,j}}{D_{II,i} + D_{II,j}} \tag{19}$$

and

$$\frac{\gamma_{cr,j}}{\gamma_{cr}} = \frac{1/D_{II,j}}{1/D_{II}} = \frac{D_{II,i}}{D_{II,i} + D_{II,j}} \tag{20}$$

Finally, the slipping displacement on i-th crack is

$$u_i = L_i \gamma_{cr,i} = L_i \frac{D_{II,j}}{D_{II,i} + D_{II,j}} \gamma_{cr} \tag{21}$$

Following the same procedure, the magnitude of a crack slip on i-th crack plane in 3D becomes

$$u_i = \sqrt{u_{i,j}^2 + u_{i,k}^2} = \sqrt{\left(L_i \frac{D_{II,j}}{D_{II,i} + D_{II,j}} \gamma_{cr,ij} \right)^2 + \left(L_i \frac{D_{II,k}}{D_{II,i} + D_{II,k}} \gamma_{cr,ik} \right)^2} \tag{22}$$

4 Constitutive laws for matrix

The current implementation allows to choose from different types of softening law, various approaches for reduction of shear stiffness (provided that cracking has been initiated), and to choose from two conditions restricting the maximum shear traction on a crack plane. This material model can be used as standalone to describe the behavior of unreinforced concrete `ConcreteFCM`, or to describe the matrix of a fiber-reinforced composite in `FRCFCM` model.

The model is described in the following sections and is summarized in Table 1.

4.1 Traction-separation law

Altogether there are 7 different options of the postpeak behavior. The choice is controlled by keyword `softType`. The particular traction-separation law becomes activated once the normal stress reaches the tensile strength f_t of concrete. The summary and the required input parameters is given in the list below.

- no softening ($softType = 0$) Material behavior is linear elastic.
- exponential softening ($softType = 1$)
  Required parameters: *Gf*, *ft*.

$$\sigma = f_t \exp(-w/w_f) \qquad \text{for } w \geq w_{\max} \tag{23}$$

$$\sigma = f_t \times \frac{w}{w_{\max}} \exp(-w_{\max}/w_f) \qquad \text{for } w < w_{\max} \tag{24}$$

$$w_f = G_f/f_t \tag{25}$$

- linear softening ($softType = 2$)
  Required parameters: *Gf*, *ft*.

$$\sigma = f_t(1 - w/w_f) \qquad \text{for } w \geq w_{\max} \tag{26}$$

$$\sigma = f_t\, w\, (w_f - w_{\max})/(w_{\max} \cdot w_f) \qquad \text{for } w < w_{\max} \tag{27}$$

$$\sigma = 0 \qquad \text{for } w_{\max} \geq w_f \tag{28}$$

$$w_f = 2G_f/f_t \tag{29}$$

- Hordijk's softening (*softType* = 3)
  Required parameters: *Gf*, *ft*.
  for $w \geq w_{\max}$:

$$\sigma = f_t \left[\left(1 + \left(\frac{c_1 w}{w_f} \right)^3 \right) \exp\left(\frac{-c_2 w}{w_f} \right) - \frac{w}{w_f} \left(1 + c_1^3 \right) \exp\left(-c_2 \right) \right] \tag{30}$$

  for $w < w_{\max}$:

$$\sigma = f_t \frac{w}{w_{\max}} \left[\left(1 + \left(\frac{c_1 w_{\max}}{w_f} \right)^3 \right) \exp\left(\frac{-c_2 w_{\max}}{w_f} \right) - \frac{w_{\max}}{w_f} \left(1 + c_1^3 \right) \exp\left(-c_2 \right) \right] \tag{31}$$

  for $w_{\max} \geq w_f$:

$$\sigma = 0 \tag{32}$$

$$w_f = 5.14\, G_f / f_t, \quad c_1 = 3, \quad c_2 = 6.93 \tag{33}$$

- user-defined with respect to crack opening (*softType* = 4)
  Required parameters: *ft*, *soft_w*, *soft(w)*.
  for $w \geq w_{\max}$ and $\text{soft\_w}_{i-1} \leq w < \text{soft\_w}_i$:

$$\sigma = f_t \left[\text{soft(w)}_{i-1} + \frac{\text{soft(w)}_i - \text{soft(w)}_{i-1}}{\text{soft\_w}_i - \text{soft\_w}_{i-1}} \left(w - \text{soft\_w}_{i-1} \right) \right] \tag{34}$$

  for $w < w_{\max}$ and $\text{soft\_w}_{i-1} \leq w_{\max} \leq \text{soft\_w}_i$:

$$\sigma = f_t \frac{w}{w_{\max}} \left[\text{soft(w)}_{i-1} + \frac{\text{soft(w)}_i - \text{soft(w)}_{i-1}}{\text{soft\_w}_i - \text{soft\_w}_{i-1}} \left(w - \text{soft\_w}_{i-1} \right) \right] \tag{35}$$

- linear hardening (*softType* = 5)
  Required parameters: *ft*, *H*, *eps_f*
  for $\varepsilon_{cr,\max} \geq eps_f$ $\sigma = 0$, otherwise

$$\sigma = \left(f_t + H\, \varepsilon_{cr,\max} \right) \frac{\varepsilon_{cr}}{\varepsilon_{cr,\max}} \tag{36}$$

- user-defined with respect to crack strain (*softType* = 6) required parameters: *ft*, *soft_eps*, *soft(eps)*

for $\varepsilon_{cr} \geq \varepsilon_{cr,\max}$ and $\text{soft\_eps}_{i-1} \leq \varepsilon_{cr} < \text{soft\_eps}_i$:

$$\sigma = f_t \left[\text{soft(eps)}_{i-1} + \frac{\text{soft(eps)}_i - \text{soft(eps)}_{i-1}}{\text{soft\_eps}_i - \text{soft\_eps}_{i-1}} \left(\varepsilon_{cr} - \text{soft\_eps}_{i-1} \right) \right] \tag{37}$$

for $\varepsilon_{cr} < \varepsilon_{cr,\max}$ and $\text{soft\_eps}_{i-1} \leq \varepsilon_{cr,\max} \leq \text{soft\_eps}_i$:

$$\sigma = f_t \frac{\varepsilon_{cr}}{\varepsilon_{cr,\max}} \left[\text{soft(eps)}_{i-1} + \frac{\text{soft(eps)}_i - \text{soft(eps)}_{i-1}}{\text{soft\_eps}_i - \text{soft\_eps}_{i-1}} \left(\varepsilon_{cr} - \text{soft\_eps}_{i-1} \right) \right] \tag{38}$$

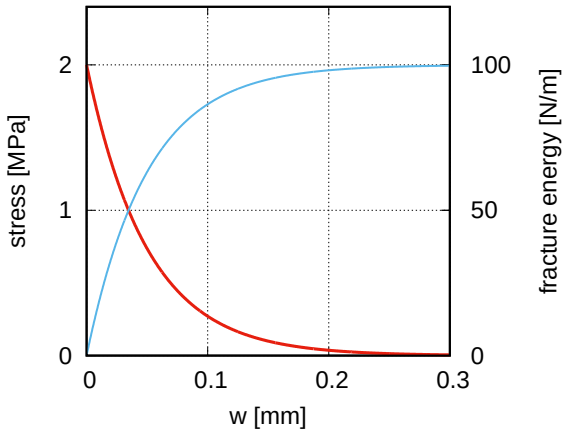

Figure 1: Traction-separation law for the exponential softening with $f_t = 2$ MPa and $G_f = 100$ N/m (`softType 1`).

4.2 Shear stiffness

The evaluation of the effective shear stiffness G_c of a cracked material is controlled by *shearType*. For *shearType* = 0 no reduction is assumed and $G_c = G$. If *shearType* = 1, a constant shear retention factor is used and

$$G_c = G \times \beta \tag{39}$$

The usually recommended value $\beta = 0.01$ is used in the case it is not user-defined (keyword *beta*).

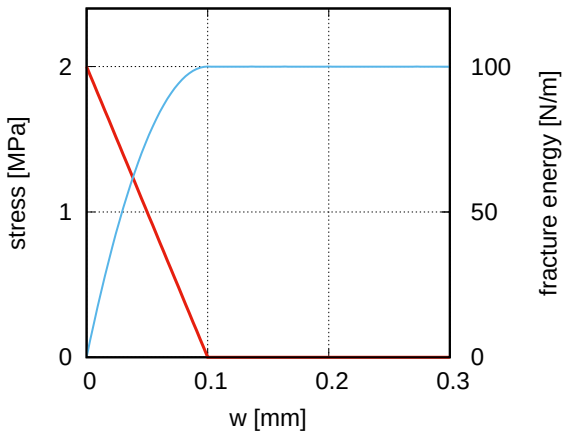

Figure 2: Traction-separation law for the linear softening with $f_t = 2$ MPa and $G_f = 100$ N/m (`softType 2`).

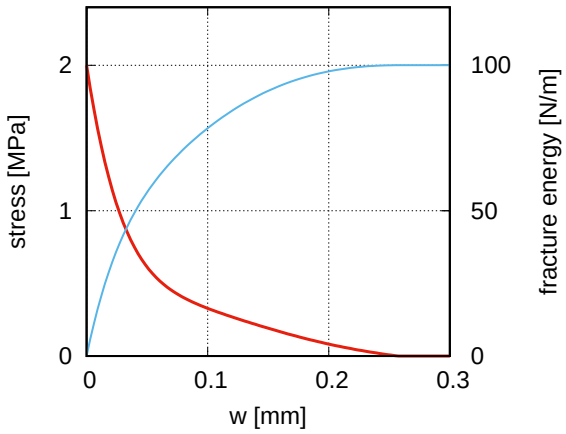

Figure 3: Traction-separation law according to Hordijk with $f_t = 2$ MPa and $G_f = 100$ N/m (`softType 3`).

With *shearType* = 2 the shear stiffness reduction is evaluated using shear factor coefficient s_F (keyword *sf*)

$$G_c = \frac{G s_F D_{cr,S}}{G + s_F D_{cr,S}} \tag{40}$$

where $D_{cr,S}$ is the normal secant stiffness of the most weakened crack. Default

value of the shear retention factor is $s_F = 20$.

Finally, if *shearType* = 3, the shear retention factor is evaluated using the user-defined piecewise linear function which depends on the maximum reached crack opening and is given by fields *beta_w* and *beta(w)*.

4.3 Shear strength

It is also possible to limit the magnitude of the resulting shear stress acting on crack plane. For *shearStrengthType* = 0 the shear stress is not limited, for *shearStrengthType* = 1 the threshold is set to the value of the tensile strength, f_t.

A more realistic limit for the shear stress is activated with *shearStrengthType* = 2; the shear stress cannot exceed the value proposed by Collins

$$\tau_{\max} = \frac{0.18\sqrt{f_c}}{0.31 + \frac{24\, w_{\max}}{a_g + 16}} \tag{41}$$

where f_c is the compressive strength in MPa, $\tau_{\max}$ is the maximum shear stress in MPa, a_g is the aggregate diameter and $w_{\max}$ is the maximum crack opening (both in mm). To use Collins' aggregate interlock in OOFEM, define *fc* in MPa, *ag* in length units of the analysis, and *lengthscale* 1 = dimensions in m, 1000 = dimensions in mm, etc. This law is depicted for several aggregate sizes and two concrete strengths in Fig. 4.

4.4 Summary

Description	Fixed crack model for concrete
Record Format	**ConcreteFCM** (in) # d(rn) # tAlpha(rn) # E(rn) # n(rn) # [ncracks(in) #] [multipleCrack-Shear] [crackSpacing(rn) #] [softType(in) #] [shearType(in) #] [shearStrengthType(in) #] [ecsm(rn) #] [Gf(rn) #] [ft(rn) #] [beta(rn) #] [sf(rn) #] [fc(rn) #] [ag(rn) #] [lengthscale(rn) #] [soft_w(ra) #] [soft(w)(ra) #] [soft_eps(ra) #] [soft(eps)(ra) #] [beta_w(ra) #] [beta(w)(ra) #] [H(rn) #] [eps_f(rn) #]
Parameters	- material model number

- *d* material density
- *tAlpha* thermal dilatation coefficient
- *E* Young's modulus
- *n* Poisson's ratio
- *ncracks* maximum allowed number of cracks
- *crackSpacing* specified distance between parallel cracks
- *multipleCrackShear* if not given, shear stiffness computed from the dominant crack, otherwise all cracks contribute
- *softType* allows to select suitable softening law:

  0 - no softening (default)
  1 - exponential softening with parameters *Gf* and *ft*
  2 - linear softening with parameters *Gf* and *ft*
  3 - Hordijk softening with parameters *Gf* and *ft*
  4 - user-defined wrt crack opening with parameters *ft*, *soft_w*, and *soft(w)*
  5 - linear hardening wrt strain with parameters *ft*, *H*, and optionally *eps_f*
  6 - user-defined wrt strain with parameters *ft*, *soft_eps*, and *soft(eps)*

- *shearType* offers to choose from different approaches for shear stiffness reduction of a cracked element

  0 - no shear reduction (default)
  1 - constant shear retention factor with parameter *beta*
  2 - constant shear factor coefficient with parameter *sf*
  3 - user-defined shear retention factor with parameters *beta_w* and *beta(w)*

	- *shearStrengthType* allows to select a shear stress limit on a crack plane 0 - no stress limit (default) 1 - constant strength = f_t 2 - Collins interlock with parameters *fc*, *ag*, and *lengthscale* - *ecsm* method used for evaluation of characteristic element size L: 1 = square root of area, 2 = projection centered, 3 = Oliver, 4 = Oliver modified, 0 (default) = projection - *Gf* fracture energy - *ft* tensile strength - *beta* shear retention factor - *sf* shear factor coefficient - *fc* compressive strength in MPa - *ag* aggregate size - *lengthscale* factor to convert crack opening and aggregate size in the case of Collins aggregate interlock; 1 = analysis in meters, 1000 = in millimeters, etc. - *soft_w* specified values of crack opening and - *soft(w)* corresponding values of traction normalized to *ft* - *soft_eps* specified values of cracking strain and - *soft(eps)* corresponding values of traction normalized to *ft* - *beta_w* specified values of crack opening and - *beta(w)* corresponding values of shear retention factor - *H* hardening modulus (expressed wrt cracking strain) - *eps_f* threshold for cracking strain after which traction is zero (applicable for linear hardening only)
Supported modes	3dMat, PlaneStress, PlaneStrain

Table 1: Fixed crack model for concrete – summary.

The following lines show a sample syntax specifying the fixed crack model with volume density 24 kN/m^3, thermal dilation coefficient 12×10^{-6} K^{-1}, Young's modulus 20 GPa, Poisson's ratio 0.2, fracture energy 100 N/m, tensile strength 2 MPa, linear softening, constant shear retention factor $\beta = 0.05$, Collins' shear strength (with compressive strength 30 MPa, aggregate size 0.01 m) and all cracks contribute to the shear stiffness; the analysis uses [m], [MPa] and [MN]:

```
ConcreteFCM 1 d 24.e-3 talpha 12.e-6 E 20000. n 0.2 Gf 100e-6 ft 2.0
softType 2 shearType 1 beta 0.05 shearStrengthType 2 fc 30 ag 0.01
lengthscale 1. multipleCrackShear
```

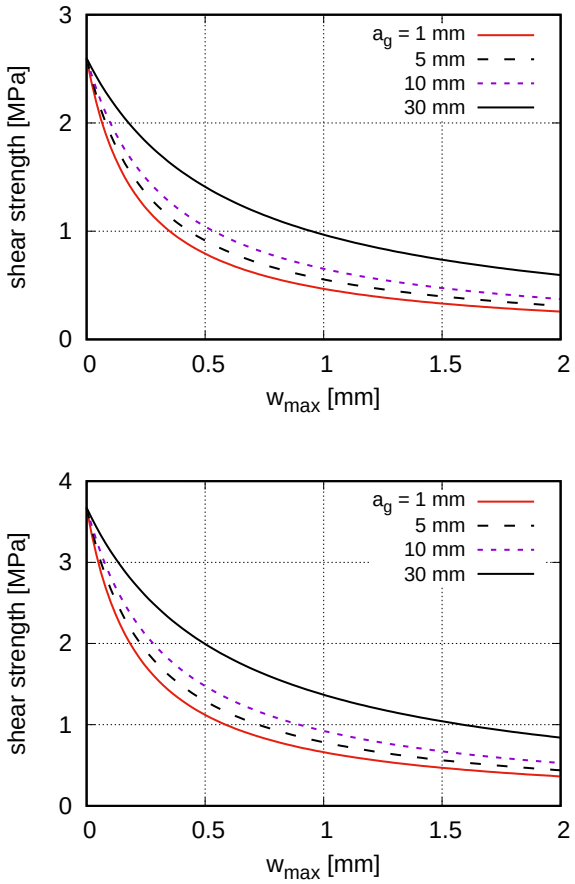

Figure 4: Dependence of the maximum shear strength on crack opening according to (41) for $f_c = 20$ MPa (top) and $f_c = 40$ MPa (bottom).

5 Constitutive laws for fibers

The presented material model for fibers cannot be used standalone but only as an extension of the `ConcreteFCM` material model called `FRCFCM` model.

It is possible to choose from three different "classes" of fibers. This choice is controlled by keyword *fiberType*: 0 = continuous aligned fibers (CAF), 1 = short aligned fibers (SAF) and 2 = short random fibers (SRF). Currently, it is not possible to combine more classes of fibers in one material model.

All of the above-mentioned fiber classes are further specified by their material properties and geometry. Fiber dosage is captured by the dimensionless volume fraction *Vf* (as decimal). All fibers are assumed to have a circular cross-section and to possess the same geometry characterized by the diameter *Df* and length *Lf* (the second parameter is applicable only for short fibers, in fiber class CAF the fibers are idealized as "infinitely" long). The last geometry-related parameter is the cross-sectional shear shape factor *kfib*, which is in the case of circular fibers equal to 0.9 (default value); this parameter plays role only in shear stiffness of an existing crack.

5.1 Influence of fiber type and orientation on V_f

Orientation of fibers with respect to the global coordinate system is for CAF and SAF controlled by parameter *orientationVector* (in the input file this vector need not be unit); for SRF the fiber orientation is random and all directions are equally probable.

Fiber orientation vector directly influences the number of fibers crossing a unit crack plane and thus the traction-separation law. For short random fibers (where the orientation is equally probable in all directions in space, not in plane), this number is

$$N = N_{tot} \int_0^{\pi/2} \int_0^{L_f/2\cos(\theta)} p_z p_\theta dz d\theta = N_{tot} \int_0^{\pi/2} \int_0^{L_f/2\cos(\theta)} \frac{2}{L_f} \sin\theta dz d\theta = \frac{N_{tot}}{2} \tag{42}$$

$$\bar{V}_{f,SRF} = V_f/2 \tag{43}$$

For continuous and short aligned fibers the effective fiber volume is

$$\bar{V}_f = V_f \cos(\theta) \tag{44}$$

where θ is the angle between the fiber axis and the crack plane normal.

Once the crack is formed, the bridging stress is transferred by both matrix and fibers.

$$\sigma_b = \sigma_{b,m} + \sigma_{b,f} \tag{45}$$

where $\sigma_{b,m}$ and $\sigma_{b,f}$ are the nominal (expressed per unit area of a crack) bridging stresses in matrix and fibers. Consequently, this relationship can be rewritten in terms of the effective stresses as

$$\sigma_b = \bar{\sigma}_{b,m}(1 - V_f) + \bar{\sigma}_{b,f}\bar{V}_f \tag{46}$$

Note that the nominal stress in fibers is obtained by multiplying the effective bridging stress in fibers by the **effective** fiber volume while the nominal stress in matrix is independent of the fiber orientation and depends entirely on the matrix volume $V_m = (1 - V_f)$. (The reason for this difference is that on one hand the number of fibers crossing an inclined plane decreases with increasing angle θ: $\bar{N} = N_{tot}\cos(\theta)$ but on the other hand with the increasing angle θ the area of the intersecting ellipse formed by the circular fiber and the crack plane grows: $\bar{A} = A/\cos(\theta)$; in the end, these two effects cancel out and the area of the matrix on the crack plane remains unaffected.)

The material of fibers is modeled as linear elastic characterized by Young's modulus E_f (*Ef* in the input record) and Poisson's ratio ν_f (*nuf*). On contrary to steel fibers, polymeric fibers are highly anisotropic and so it makes much more sense to define the combination of Young's modulus and the fiber shear modulus G_f (*Gfib*) (which appears only in the expression for the crack shear stiffness).

5.2 Overall elastic stiffness

The overall elastic stiffness of the fiber-reinforced composite is calculated for all three classes of fibers as a weighted average of the two Young's moduli

$$E = V_f E_f + (1 - V_f)E_m \tag{47}$$

The Poisson ratio is considered to be equal to Poisson's ratio of the matrix. This simplification is not exact but is sufficient for the present purpose. What is important is that it allows to use linear isotropic material in the elastic region.

5.3 Crack initiation

Similarly to `ConcreteFCM`, cracking is initiated once the tensile stress σ in matrix reaches the tensile strength f_t. If the material is undamaged, this tensile stress is

calculated from the maximum principal stress $\sigma = \sigma_1$. Criterion for the second crack in 3D or plane strain is evaluated from the maximum tensile stress in the crack plane. Finally, in the case of the second crack in plane stress or (3rd crack in 3D), the tensile stress is evaluated in the perpendicular direction to the first (and second) crack.

Before the onset of cracking the strains in the matrix and fibers can be treated as mutually compatible and equal to the deformation of the composite

$$\varepsilon = \varepsilon_f = \frac{\bar{\sigma}_f}{E_f} = \varepsilon_m = \frac{\bar{\sigma}_m}{E_m} \tag{48}$$

In this simplified evaluation, the normal stress in the composite is the sum of the effective stresses multiplied by their volume ratio

$$\sigma = (1 - V_f)\bar{\sigma}_m + V_f\bar{\sigma}_f = \bar{\sigma}_m\,(1 - Vf + VfE_f/E_m) \tag{49}$$

from which the effective stress in matrix can be expressed as

$$\bar{\sigma}_m = \frac{\sigma}{1 - V_f\,(E_f/E_m - 1)} \tag{50}$$

5.4 Pull-out of a single fiber

If a fiber is bridging a crack, then the bridging force transferred by the fiber F_b must be equal to an anchoring force F_a. This model assumes that the entire anchoring force stems from the frictional bond stress between the fiber outer surface and matrix. This stress becomes activated once the fiber starts to be pulled out and the displacements of the fiber and matrix cease to be compatible. A chemical bond is neglected.

The anchoring force can be computed as

$$F_a = F_0 \exp(f\theta) \tag{51}$$

where F_0 is the resultant of the bond shear stress τ_s between the fiber and matrix and f is a snubbing coefficient. This factor depends on the material of fibers and captures an additional increase in the anchoring force of fibers which are not oriented in the normal direction to the crack plane. In the special case when $f = 0$, the fiber is pulled out over a non-frictional pulley and $F_a = F_0$.

The distribution of the bond stress τ_s is assumed to be uniform on the fiber surface and therefore its resultant can be computed as

$$F_0 = \pi D_f a \tau_s \tag{52}$$

where a is the length of the zone where the fiber is debonded from the matrix. If the debonded zone is smaller than the embedded length of the fiber, the relative displacements of the fiber and matrix are negligible and τ_s can be treated as constant $\tau_s = \tau_0$. The debonded zone starts developing at the crack plane and continues growing towards both ends of the fiber equally until it reaches the closer tip. At this instant the shorter part of the fiber starts "sliding" and the embedded length is decreasing. The transitional crack opening at which the debonding has ceased and all fibers are being pulled out is denoted as w^* and can be analytically derived as

$$w^* = \frac{L_f^2 \tau_0}{(1+\eta) E_f D_f} \tag{53}$$

where

$$\eta = \frac{E_f V_f}{E_m (1 - V_f)} \tag{54}$$

Larger pull-out displacements can lead to significant physical changes in the fiber surface which can result into changes in the bond shear stress. This phenomenon is captured by function $\tau_s(w)$ relating the frictional bond to the crack opening and is implemented in three alternative formulations. (In order to keep $\tau_s(w) = \tau_0$ use *fssType* $= 0$.) In conventional FRC with ordinary concrete matrix, the frictional bond usually decreases with increasing slip. This is captured by a function proposed by Sajdlová (*fssType* $= 1$):

$$\tau_s(w) = \tau_0 \left[1 + \mathrm{sign}(b_0) \left(1 - \exp\left(-\frac{|b_0| w}{D_f} \right) \right) \right] \tag{55}$$

where b_0 is a micromechanical parameter. In composites with high-strength matrix and coated high-strength steel fibers (HSFRC, UHPFRC) as well as in SHCC materials with polymeric fibers, the frictional bond-slip relation often exhibits hardening; this phenomenon can be well approximated by a cubic function (activated with *fssType* $= 2$) proposed by Kabele

$$\tau_s(w) = \tau_0 \left[1 + b_1 \frac{w}{D_f} + b_2 \left(\frac{w}{D_f} \right)^2 + b_3 \left(\frac{w}{D_f} \right)^3 \right] \tag{56}$$

or an alternative formulation which results in smooth changes in F_0 (activated with *fssType* $= 3$)

$$\tau_s(w) = \tilde{\tau}_0 + \tau_0 \left[b_1 \frac{\tilde{w}}{D_f} + b_2 \left(\frac{\tilde{w}}{D_f} \right)^2 + b_3 \left(\frac{\tilde{w}}{D_f} \right)^3 \right] \tag{57}$$

In the last two equations b_1, b_2 and b_3 are micromechanical parameters and additionally in the last equation $\tilde{w} = w - w^*$, $\tilde{\tau_0} = \tau_0(1. - w^*/L_f)^{-2}$ for SRF and $\tilde{\tau_0} = \tau_0 E_f(1+\eta)D_f/[E_f(1+\eta)D_f - 2L_f\tau_0]$ for SAF.

5.5 Traction-separation law for fibers

This section presents traction-separation laws for CAF, SAF and SRF classes of fibers as well as the expressions for the secant and tangent stiffnesses. All these expressions are formulated with respect to crack opening w.

The formulae given in the literature and presented also in the preceding sections were derived under the assumption that the crack surface is perfectly straight. However, owing to the presence of fibers which bridge the crack, the surface can become distorted. The source of this deformation can be sought in the shear stresses in the bond between the matrix and fibers. Crack opening is increasing with the distance from the bridging fibers. In the vicinity of a fiber the crack opening is smaller and therefore the actual pull-out displacement of a fiber is smaller than the average crack opening. To capture this phenomenon, the average crack opening is replaced by the "effective crack opening" $\bar{w}$ defined as

$$\bar{w} = w - \Delta w = L\varepsilon_{cr} - \Delta w \tag{58}$$

where Δw is a parameter defined by keyword *fibreActivationOpening*. This parameter can be imagined as a "lag" of the fiber-related crack opening behind the matrix-related crack opening.

One obstacle present in all traction-separation laws is the infinite derivative at $\bar{w} = 0^+$ which can easily spoil convergence if $\Delta w > 0$. To overcome this problem the traction-separation law can be smoothed near $w = \Delta w$ by a third-order polynomial. The resulting function is then continuous in values and first derivatives. This smoothing starts at $w = \Delta w - \Delta w_0$ and terminates at $w = \Delta w + \Delta w_1$ where Δw_0 and Δw_1 are positive parameters (in the input record *dw0* and *dw1*, default value is zero). This smoothing technique is demonstrated in Fig. 5.

Another simplification present in the derivation is that the matrix is ideally brittle and in the crack does not transfer any stresses which is not true in the case of the cohesive crack. However, it turns out that the arising differences are very small (less than 1%). The formula for the traction separation law and continuous aligned fibers derived under the assumption that the crack surfaces transfer traction is for the purpose of comparison presented in the following

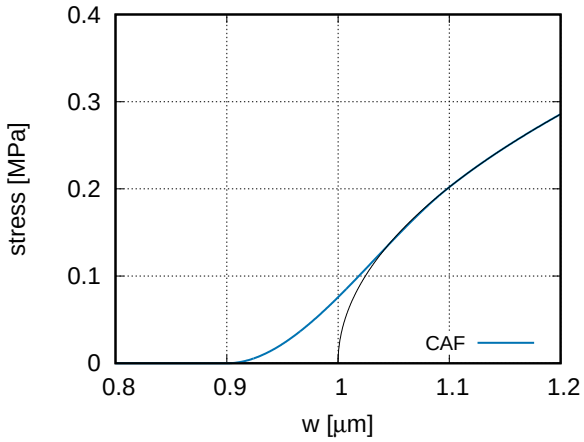

Figure 5: Original and smoothed traction-separation law for CAF fibers; $\Delta w = 1$ μm, smoothing from 0.9 to 1.1 μm.

section.

5.5.1 Continuous Aligned Fibers (CAF)

The nominal bridging stress (as well as stiffness) of the aligned fibers which are not perpendicular to the crack plane $\sigma_{b,f,\theta}$ can be very easily obtained by multiplying the nominal bridging stress of fibers perpendicular to crack $\sigma_{b,f}$ by two terms: the first one reflecting lower volume of inclined fibers passing through the crack plane and the second one capturing the snubbing effect:

$$\sigma_{b,f,\theta} = \bar{\sigma}_{b,f}\bar{V}_f \exp(\theta f) = \sigma_{b,f}\cos(\theta)\exp(\theta f) \tag{59}$$

For the continuous aligned fibers perpendicular to crack, the nominal bridging stress can be derived as

$$\sigma_{b,f} = 2V_f\sqrt{\frac{E_f(1+\eta)\tau_0}{D_f}\,\bar{w}} \tag{60}$$

If the influence of the normal traction transferred by matrix is not neglected, an additional term which is negligible compared to the first one and is decreasing with crack opening appears in the expression for the bridging stress.

$$\sigma_{b,f} = V_f\left(2\sqrt{\frac{E_f(1+\eta)\tau_0}{D_f}\,\bar{w}} + \bar{\sigma}_{b,m}\frac{E_f}{E_m}\right) \tag{61}$$

Tangent stiffness in the normal direction of the cohesive crack is then the partial derivative of (60) with respect to cracking strain

$$D_{I,T} = \frac{\partial \sigma_{b,f}}{\partial \varepsilon_{cr}} = V_f L \sqrt{\frac{E_f(1+\eta)\tau_0}{D_f \bar{w}}} \tag{62}$$

5.5.2 Short Aligned Fibers (SAF)

The constitutive equation describing the normal bridging stress carried by short aligned fibers has a different form when some fibers undergo debonding and some pullout and when all fibers are being pulled out. A transition between these two modes is defined by the the opening displacement w^* (53). Note that these two functions do not have to be continuous in values - this depends on the choice of $\tau_s(w)$.

$$\sigma_{b,f}(w) = 2V_f \sqrt{\frac{E_f(1+\eta)\tau_0 \bar{w}}{D_f}} - \frac{V_f E_f (1+\eta)\bar{w}}{L_f} \quad \text{for } \bar{w} < w^* \tag{63}$$

$$\sigma_{b,f}(w) = \frac{V_f L_f \tau_s(w)}{D_f}\left(1 - \frac{2\bar{w}}{L_f}\right)^2 \quad \text{for } w^* \le \bar{w} < L_f/2 \tag{64}$$

$$\sigma_{b,f}(w) = 0 \quad \text{for } \bar{w} > L_f/2 \tag{65}$$

Tangent stiffness can be expressed as

$$D_{I,T}(w) = V_f L \left(\sqrt{\frac{(1+\eta)E_f \tau_0}{D_f \bar{w}}} - \frac{(1+\eta)E_f}{L_f} \right) \quad \text{for } \bar{w} < w^* \tag{66}$$

$$D_{I,T}(w) = -\frac{4V_f \tau_s(w) L}{D_f}\left(1 - \frac{2\bar{w}}{L_f}\right) \quad \text{for } w^* \le \bar{w} < L_f/2 \tag{67}$$

$$D_{I,T}(w) = 0 \quad \text{for } \bar{w} > L_f/2 \tag{68}$$

5.5.3 Short Random Fibers (SRF)

Similarly to SAF the constitutive equations and tangent stiffnesses are expressed separately for $w \lessgtr w^*$:

$$\sigma_{b,f}(w) = \frac{gV_f L_f \tau_0}{2D_f}\left(2\sqrt{\frac{\bar{w}}{w^*}} - \frac{\bar{w}}{w^*}\right) \quad \text{for } \bar{w} < w^* \tag{69}$$

$$\sigma_{b,f}(w) = \frac{gV_f L_f \tau_s(w)}{2D_f}\left(1 - \frac{2w}{L_f}\right)^2 \quad \text{for } w^* \le \bar{w} < L_f/2 \tag{70}$$

$$\sigma_{b,f}(w) = 0 \quad \text{for } \bar{w} > L_f/2 \tag{71}$$

$$D_{I,T}(w) = \frac{gV_f L_f \tau_0 L}{2D_f w^*}\left(\frac{1}{\sqrt{\frac{\bar{w}}{w^*}}} - 1\right) \quad \text{for } \bar{w} < w^* \tag{72}$$

$$D_{I,T}(w) = D_{I,T} = -\frac{4gV_f \tau_s(w) L}{2D_f}\left(1 - \frac{2\bar{w}}{L_f}\right) \quad \text{for } w^* \le \bar{w} < L_f/2 \tag{73}$$

$$D_{I,T}(w) = 0 \quad \text{for } \bar{w} > L_f/2 \tag{74}$$

Here, g is the snubbing factor defined as

$$g = 2\frac{1 + \exp(\pi f/2)}{4 + f^2} \tag{75}$$

5.5.4 Unloading and reloading

Compared to the bridging stress in matrix, the stress in fibers does not decrease linearly to origin when the crack is unloading. Current implementation uses a power function

$$\sigma_{b,f}(w) = \sigma_{b,f}(w_{max})\left(\frac{\bar{w}}{\bar{w}_{max}}\right)^M \tag{76}$$

where $w_{\max}$ is the maximum crack width reached in the entire previous history and M is a positive constant, its default value is $M = 4$. See Fig. 6 for an example of the unloading and reloading paths with $M = 4$.

The tangent stiffness for unloading and reloading is then

$$D_{I,T} = \sigma_{b,f}(w_{max})\frac{ML}{\bar{w}_{max}}\left(\frac{\bar{w}}{\bar{w}_{max}}\right)^{M-1} \tag{77}$$

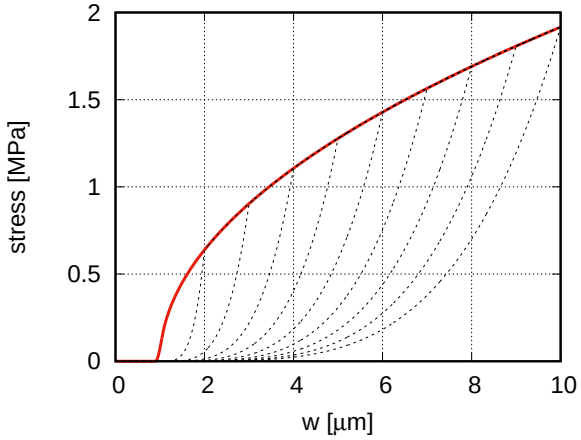

Figure 6: Unloading and reloading paths of the fiber reinforcement (nominal stress, continuous aligned fibers, $\Delta w = 1$ μm).

5.6 Crack shearing

The influence of crack opening and sliding on the bridging shear stress carried by fibers is expressed as

$$\tau_{b,f} = \bar{V}_f k G_f \frac{u}{w_{max}} = \frac{\bar{V}_f k G_f}{\varepsilon_{cr,max}} \gamma_{cr} = D_{II,f} \gamma_{cr} \tag{78}$$

where $\bar{V}_f$ is the effective volume of fibers crossing a crack plane ($V_f/2$ for SRF and $V_f \cos(\theta)$ for CAF and SAF), k is the fiber cross-section shape correction factor and G_f is the fiber shear modulus. This expression is motivated by hypothesis that the fibers bridging the crack planes behave as the Timoshenko beams subjected to shear. Note that the shear stiffness of fibers is not recovered upon unloading.

5.7 Damage of bridging fibers caused by crack shearing

It has been found, both by numeric simulations and experiments, that in some high performance fiber reinforced cement composites, especially SHCC with polymeric fibers, fibers rupture when cracks are exposed to shearing. This phenomenon is modeled by damage parameter ω, which accounts for the ratio of ruptured fibers and varies between the values of 0 and 1: $\omega = 0$ means that

no fibers ruptured while $\omega = 1$ indicates rupture of all bridging fibers. It is assumed that ω depends on the maximum shear strain sustained by the protruding portions of bridging fibers throughout the loading history. This strain can be expressed as:

$$\gamma_{f,max} = \max\left(\frac{|u_i(t)|}{\max\left(w_i(t)\right)}\right) \quad \ldots w(t) > \Delta w \tag{79}$$

where u_i is the crack sliding displacement (CSD) and and w_i is the maximum value of the crack opening displacement of the i-th crack. This means that the damage does not grow if the crack closes (crack opening decreases). If more cracks exist, the maximum contribution is considered.

Two different one-parameter damage evolution laws are currently implemented. For $fDamType = 0$ the damage is deactivated, with $fDamType = 1$ damage is described by

$$\omega(\gamma_f) = \min\left(\frac{\gamma_f}{\gamma_{fc}},\, 1\right) \tag{80}$$

and finally with $fDamType = 2$

$$\omega(\gamma_f) = 1 - \exp\left(-\frac{\gamma_f}{\gamma_{fc}}\right) \tag{81}$$

where γ_{fc} (*gammaCrack* in the input record) is a material parameter. The two functions are shown in Fig. 7.

A special care must be given to a case with small opening which can easily result into complete loss of integrity (complete damage). Since damage reduces the number of crack-bridging fibers, which is proportional to the fiber volume fraction, its effect can be suitably implemented by introducing the effective volume fraction

$$V_f^* = V_f(1 - \omega) \tag{82}$$

which results into modifications of the traction-separation relationship

$$\sigma_{b,f,\omega} = \sigma_{b,f}(1 - \omega) \tag{83}$$

and both normal and shear crack stiffness

$$D_{I,f,\omega} = D_{I,f}(1 - \omega) \tag{84}$$

$$D_{II,f,\omega} = D_{II,f}(1 - \omega) \tag{85}$$

The decrease in fiber volume is assumed to be the same for all crack planes, independently of fiber type and fiber orientation (for CAF and SAF).

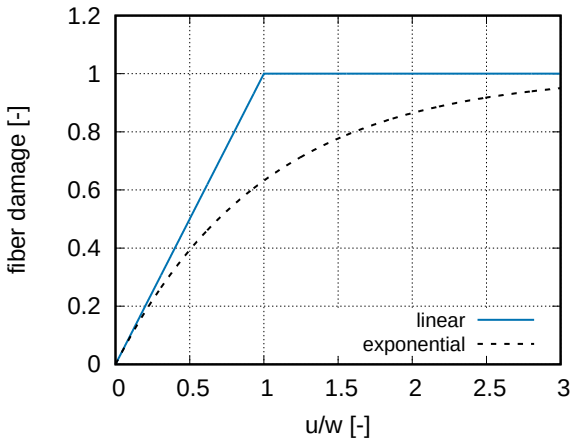

Figure 7: Evolution of fiber damage according to equations (80) and (81); parameter γ_{fc} is in both cases set equal to 1 and $\Delta w = 0$.).

6 Composite bridging model

6.1 Bridging stress and crack stiffness

For stresses below the strength limit, the behavior of the composite is not characterized entirely by the matrix, even though its contribution is dominant. The elastic stiffness matrix is constructed from the overall elastic stiffness (47) and from Poisson's ratio of the matrix. Once the principal stress in the matrix exceeds its tensile strength, the traction across the crack is transferred jointly by matrix and fibers.

Total composite normal bridging traction σ_b is obtained by summing up the (nominal) contribution from matrix $\sigma_{b,m}$ and fibers $\sigma_{b,f}$. The normal traction is equal to the normal stress σ

$$\sigma_b = \sigma_{b,m} + \sigma_{b,f} = \bar{\sigma}_{b,m}(1 - V_f) + \bar{\sigma}_{b,f}\bar{V}_f = \sigma \tag{86}$$

Similarly, the shear stress must be equal to shear traction which is the sum of two components: shear traction transferred by the matrix and by fibers

$$\tau_b = \tau_{b,m} + \tau_{b,f} = \tau \tag{87}$$

In these two equations, all bridging stresses are functions of a crack opening w (displacement normal to crack plane) and crack sliding u (displacement in direction of the crack plane).

The normal and shear stiffness of the i-th crack is a sum of the individual nominal normal stiffnesses

$$D_{I,i} = D_{I,f,i} + D_{I,m,i} \tag{88}$$

$$D_{II,i} = D_{II,f,i} + D_{II,m,i} \tag{89}$$

The nominal stiffnesses of matrix D_m is a product of the effective stiffness and $(1 - V_f)$ while the nominal stiffness of fibers D_f is a product of the effective stiffness and $\bar{V}_f$.

One example of the dependence of the total bridging stress on the crack opening is shown in Fig. 8; it was computed with short random fibers and both short and long aligned fibers oriented perpendicular to the crack surface, $E_m = 20$ GPa, $f_t = 2$ MPa, $G_f = 5$ N/m, exponential softening, $E_f = 20$ GPa, $V_f = 0.02$, $D_f = 40$ μm, $L_f = 12$ mm, $\tau_0 = 0.5$ MPa, $f = 0.5$, fiber activation opening 1 μm, smooth transition from 0.9 to 1.1 μm.

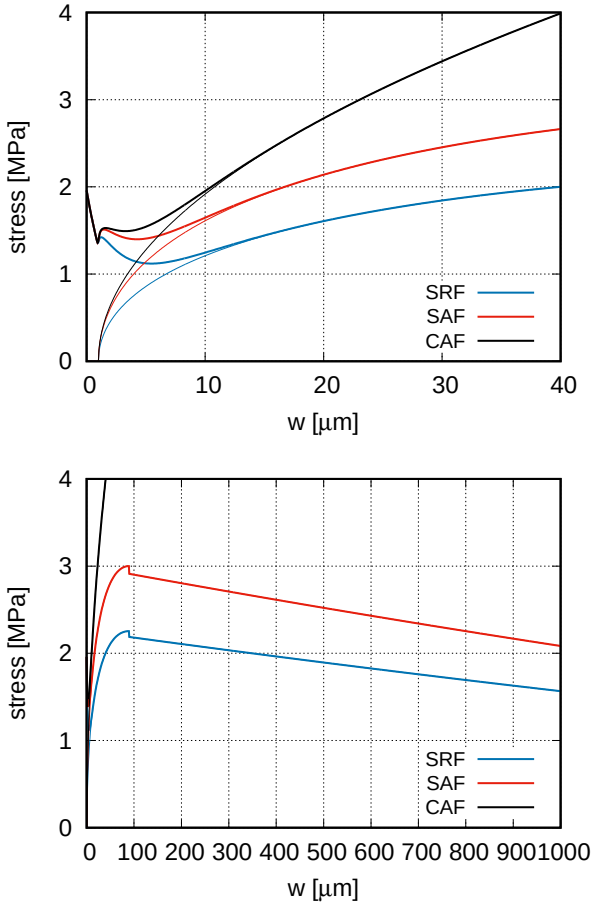

Figure 8: Total bridging stress (thick curves) and fiber bridging stress (thin curves) for CAF, SAF and SRF classes computed with fiber activation opening 1 μm and a smooth transition (thick curves only).

6.2 Crack-spacing

In the simulations of specimens and structures made of fiber reinforced composites it can become convenient to use a finite element mesh with nonuniform size of finite elements. Four different cases need to be considered: 2 for material which exhibits tension softening and 2 other for material with strain hardening.

If the material exhibits **tension-softening** and the finite **element size is small** – less than the real distance between cracks – no special treatment needs to be employed. For material with **strain-softening**, mesh with **bigger ele-**

ments and the material exhibits multiple cracking (e.g. reinforced concrete), it is essential to introduce user-defined crack spacing. This procedure preserves objectivity by assuming that more parallel cracks can develop in one element. The crack spacing distance is controlled by keyword *crackSpacing*.

To guarantee a smooth transition, the number of parallel cracks, which can develop in one element, is not an integer; it is defined as

$$N_{cr} = 1 \quad \ldots \text{if crack spacing} \geq L \tag{90}$$

$$N_{cr} = \frac{L}{\text{crack spacing}} \quad \ldots \text{if crack spacing} < L \tag{91}$$

This number of fictitious parallel cracks N_{cr} is then used to compute the adjusted element size $\hat{L} = L/N_{cr}$ in the crack-band approach. Additionally, the number of parallel cracks N_{cr} is utilized in computing the effective crack opening $\hat{w} = w/N_{cr}$, and slip $\hat{u} = u/N_{cr}$ which appear in the traction-separation and damage evolution laws. Moreover, more than one parallel cracks lead to reduction in the overall normal and shear stiffnesses. The normal stiffness is both for matrix and fibers derived for the effective crack opening *hatw* and the total stiffness is then divided by the number of parallel cracks to reflect that the crack stiffnesses are connected in series.

$$\hat{D}_I = D_I(\hat{w})/N_{cr} \tag{92}$$

Similar formula holds also for the shear stiffness of matrix:

$$\hat{D}_{II,m} = D_{II,m}(\hat{w})/N_{cr} \tag{93}$$

Interestingly, the shear stiffness of fibers is independent of the number of parallel cracks (of course except for the effect of damage ω which depends on the ratio $\hat{u}/\hat{w}$).

The crack spacing at the crack saturation state can be for the **strain-hardening** materials derived analytically. This distance depends on the fiber type, fiber volume quantity, length and diameter, matrix tensile strength, strength of the bond between fiber and matrix, and snubbing.

$$x_{CAF} = \frac{(1 - V_f)\, f_t D_f}{4 V_f \tau_0} \tag{94}$$

$$x_{SAF} = 0.5\sqrt{L_f^2 - 4 L_f x_{CAF}} \tag{95}$$

$$\lambda = \frac{2}{\pi} \frac{4 + f^2}{1 + \exp(\pi f/2)} \tag{96}$$

$$x_{SRF} = \frac{1}{2}\left(L_f - \sqrt{L_f^2 - 2\pi L_f \lambda x_{CAF}}\right) \tag{97}$$

If the element size is **larger** than the computed crack spacing, the same treatment as for the strain-softening materials should be employed. In order to the activate automatic evaluation of the crack spacing use string *computeCrackSpacing* instead of *crackSpacing*. On contrary to this, the **finer finite element** mesh calls for the nonlocal approach described in Section 7.

The material parameters are summarized in Tables 1 (matrix) and 2 (fiber extension).

Description	Fixed crack model for FRC
Record Format	**FRCFCM** input record of ConcreteFCM $Vf_{(rn)}$ # $Lf_{(rn)}$ # $Df_{(rn)}$ # $Ef_{(rn)}$ # [$nuf_{(rn)}$ #] [$Gfib_{(rn)}$ #] [$kfib_{(rn)}$ #] $tau\_0_{(rn)}$ # [$b0_{(rn)}$ #] [$b1_{(rn)}$ #] [$b2_{(rn)}$ #] [$b3_{(rn)}$ #] $f_{(rn)}$ # [$M_{(in)}$ #] [fibreOrientationVector$_{(ra)}$ #] [$fssType_{(in)}$ #] [$fDamType_{(in)}$ #] [$fiberType_{(in)}$ #] [$gammaCrack_{(rn)}$ #] [computeCrackSpacing] [$fibreActivationOpening_{(rn)}$ #] [$dw0_{(rn)}$ #] [$dw1_{(rn)}$ #]
Parameters	- *Vf* fiber content expressed as decimal - *Lf* fiber length - *Df* fiber diameter - *Ef* fiber Young's modulus - *nuf* fiber Poisson's ratio - *Gfib* fiber shear modulus (read when *nuf* is not provided) - *kfib* fiber cross-sectional shape correction factor - *tau_0* bond shear strength at zero slip - *b0* micromechanical parameter for fiber shear according to Sajdlová - *b1*, *b2*, *b3* micromechanical parameter for fiber shear according to Kabele - *f* snubbing friction coefficient - *M* exponent related to fiber unloading - *fibreOrientationVector* vector specifying orientation for CAF and SAF fibers

- *fssType* type of Fiber bond Shear Strength (bond shear strength vs. crack opening)

  0 - constant shear strength
  1 - bond shear strength with parameter *b0*
  2 - bond shear strength with parameters *b1*, *b2*, *b3*
  3 - bond shear strength with parameters *b1*, *b2*, *b3* which leads to smooth traction-separation law

- *fDamType* type of damage law for fibers

  0 - no damage
  1 - damage controlled by shear slip deformation of the crack (with *gammaCrack*), linear law
  2 - damage controlled by shear slip deformation of the crack (with *gammaCrack*), exponential law

- *fiberType* class of reinforcing fibers

  0 - CAF (continuous aligned fibers)
  1 - SAF (short aligned fibers)
  2 - SRF (short randomly oriented fibers)

- *gammaCrack* crack shear strain parameter applicable with fDamType = 1 or 2 (here the crack shear strain is understood as the crack slip u divided by the crack opening w)
- *computeCrackSpacing* crack spacing is evaluated automatically based on defined composition
- *fibreActivationOpening* crack opening at which the fibers begin transferring bridging stress

	- *dw0*, *dw1* applicable only if *fibreActivationOpening* $\neq 0$, then it allows to smoothen the traction-separation law for fibers; lower bound is *fibreActivationOpening* - *dw0* and the upper bound is *fibreActivationOpening* - *dw1*
Supported modes	3dMat, PlaneStress, PlaneStrain

Table 2: Fixed crack model for fiber reinforced concrete – summary.

The following lines show a sample syntax for material with fixed cracks reinforced by continuous aligned fibers with volume density 24 kN/m^3, thermal dilation coefficient 12×10^{-6} K^{-1}, Young's modulus of the matrix 20 GPa, Poisson's ratio of matrix 0.2, fracture energy of matrix 100 N/m, tensile strength of matrix 2 MPa, linear tension softening, constant shear retention factor $\beta = 0.05$, unlimited shear strength (`shearStrengthType = 0`), continuous aligned fibers, fiber volume $V_f = 2\%$, fiber diameter $D_f = 0.04$ mm, Young's modulus of fibers $E_f = 20$ GPa, shear modulus of fibers $G_f = 1$ GPa, fiber-matrix bond strength $\tau_0 = 1$ MPa, snubbing coefficient $f = 0.7$, shear correction coefficient $k = 0.9$, deactivated fiber damage, fiber act if COD exceeds 10 μm (with smoothing from $w = 8to11$ μm), fiber orientation at 45 degrees in x-y plane, automatic evaluation of crack spacing from composition; the analysis uses [m], [MPa] and [MN]:

```
FRCFCM 1 d 24.e-3 talpha 12.e-6 E 20000. n 0.2 Gf 100e-6 ft 2.0
softType 2 shearType 1 beta 0.05 FiberType 0 Vf 0.02 Df 0.04e-3
Ef 20000. Gfib 1000. tau_0 1. FSStype 0 f 0.7 kfib 0.9 fDamType 0
fibreactivationopening 10.e-6 dw0 2.e-6 dw1 1.e-6 orientationVector
3 1. 1. 0. computeCrackSpacing
```

7 Nonlocal model for SHCC

As already mentioned in Sections 2 and 6.2, the local model FRCFCM must not be used for cementitious materials which exhibit strain hardening. If it is used, then the results will become strongly dependent on the density of the finite element mesh as the damage would tend to localize into all elements in the critical region. The more uniform is the loading (e.g. direct tension, four point bending), the more the results become influenced by the size of the finite elements. This behavior is demonstrated later in Sections 9 and 10.

The experiments indicate that in SHCC the cracks tend to localize into a pattern with a characteristic length – the crack spacing distance. This distance can be under certain simplifications derived analytically; it depends on not only on the properties and the class of fibers and matrix but also on the strength of the interfacial bond and on the snubbing friction should the fibers be oriented at an inclined angle with respect to the crack. The crack spacing distance is for different fiber classes given by equations (94)-(97).

The crack initiation criterion as well as the mutual interaction between cracks is in this model established by a new concept based on a "nonlocal" fiber stress.

7.1 Conceptual idea of nonlocal fiber stress

In a uniaxial tensile test, the resultant of a stress transferred by a crack must be equal to the loading forces acting at the ends of the specimen as well as to a stress resultant created in an arbitrary section. A schematic representation of this test is shown in Figure 9. The stress σ which initiated cracking and produced its opening w must be in equilibrium with the sum of the nominal bridging stresses (without bars, see the bottom picture in Fig. 9) in fibers and matrix (45). The nominal stress can be computed as the effective stress (with bars, see the top picture in Fig. 9) multiplied by the (*effective*) volume fraction. Up to a distance a from the crack, the displacements of the matrix and fibers are not compatible, the fibers are debonded; this gives rise to the frictional bond stress τ. The resultant of the bond stresses acting on a single fiber is in equilibrium with the resultant of the effective bridging stress $\bar{\sigma}_{b,f}$. If the magnitude of the bridging bond stress is independent of the bond slip and the fibers are aligned and perpendicular to the crack, the stress in fibers is diminishing linearly with the distance from the crack until $x = a$. At $x = a$ the displacements become compatible and so the value of the nominal stress is a constant depending on the deformation, Young's moduli of the matrix and fibers and the volume fraction of fibers.

The "nonlocal" fiber stress mentioned earlier is in fact the nominal stress in fibers σ_f which is evaluated from the bridging stress and the distance from the crack. This stress then plays a significant role in the criterion for the crack initiation (105) because, as shown in the bottom part of Fig. 9, σ is split in the investigated cross-section into $\sigma_f = \sigma_{NL}$ and σ_m. Providing that $x < a$, then the resulting effective stress in matrix (which is compared to the tensile strength f_t) is way lower than according to (50). Similarly, if the distance between two cracks is smaller than a, then the bridging stresses in fibers start interacting.

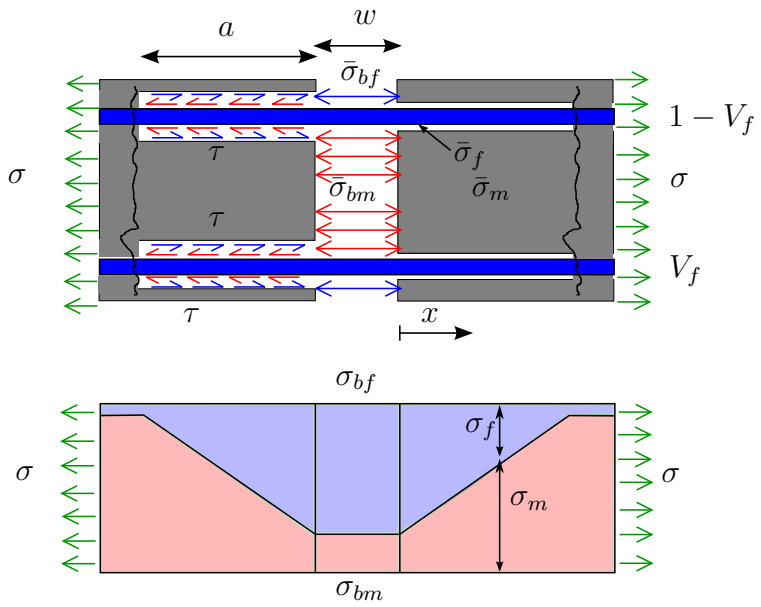

Figure 9: A schematic depiction of nominal and effective stresses in matrix and fibers at the vicinity of a crack. For $x \leq a$, where a is the length of the debonded zone (98), the effective stress in the matrix $\bar{\sigma}_m$ is computed from equation (105).

7.2 Evaluation of nonlocal stress

The nominal value of nonlocal stress σ_{NL} at a certain distance from the "source" crack is influenced by several factors. The key component is the effective value of the bridging stress $\bar{\sigma}_{b,f}$ transferred by the fibers in the target crack; the value of this stress must be high enough to cause debonding of fibers from the matrix in the region where the nonlocal stress is evaluated. If the nonlocal stress is

evaluated outside the debonded zone, it is zero (because the strains in matrix and fibers are compatible and hence no "prestress" in fibers can develop).

To compute the nonlocal stress in fibers σ_{NL} is very computationally demanding because it is evaluated in all integration points in all elements which are in a vicinity of a crack; this distance is characterized by the nonlocal radius r. In the case of the short fibers r cannot exceed half of the fiber length; in the case of long fibers (CAF), r depends on the fiber diameter and bond friction and can be roughly estimated as (94).

Compared to typical nonlocal models in which the nonlocal quantity at a certain point is computed as a nonlocal average in nonlocal radius r, here the nonlocal stress in fibers σ_{NL} is taken as the maximum contribution.

The nonlocal stress is calculated from the nominal value of the fiber bridging stress which is subsequently reduced to take into account

- friction at the crack surface (idealized to behave as a frictional pulley) provided that the fibers are randomly oriented or in the case of aligned fibers the orientation is not aligned with the crack normal
- bond friction between the fiber surface and matrix
- angle ϕ between the normal vector of the target crack (or the principal stress vector) and the fiber orientation vector (CAF, SAF) or normal vector of the source crack (SRF).

The computed length of the zone a (where the fiber is debonded from the matrix) is independent of the fiber class as well as on the angle between the fiber and the crack normal. Under certain assumptions and simplifications this distance can be derived as

$$a = \sqrt{\frac{E_f D_f \Delta}{2\tau_0(1+\eta)}} \tag{98}$$

where Δ is the pull-out displacement. If the composite contains short fibers and should the debonded length according to (98) exceed $L_f/2$, then a is set to $L_f/2$. This function is shown for typical values of material parameters in Fig. 10. However, this does not mean that the length of the debonded zone is the same for different classes of fibers and the same bridging stress.

Friction of fibers at the crack surface (captured by snubbing coefficient f) as well as their increasing inclination increase the bridging stress $\sigma_{b,f}$ but also the

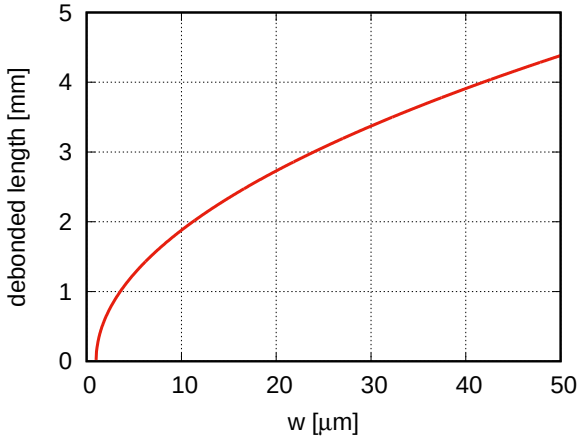

Figure 10: Dependence of the debonded length on crack opening evaluated according to (98) with $E_f = E_m = 20$ GPa, $D_f = 40$ μm, $\tau_0 = 0.5$ MPa and fiber activation opening 1 μm.

difference between the bridging stress and the stress in fibers just behind the crack surface $\sigma_f(0) = \sigma_{f,0}$ which can be derived as

$$\sigma_{f,0} = \frac{2}{3g}\sigma_{b,f} \quad \dots \text{for SRF} \tag{99}$$

$$\sigma_{f,0} = \frac{1}{\cos(\theta)\exp(f\theta)}\sigma_{b,f} \quad \dots \text{for CAF and SAF} \tag{100}$$

where θ is the angle between the fiber orientation vector and the crack normal. This normal stress is oriented in direction of the crack normal in the case of random fibers and in direction of fibers in the case of aligned fibers.

Consequently, the fiber stress is decreasing with distance from the crack and the source stems from the bond friction. The cumulative decrease is denoted as $\Delta\sigma_f$ and can be expressed as

$$\Delta\sigma_f(x) = \frac{4V_f\tau_0 x}{D_f} \quad \dots \text{for CAF} \tag{101}$$

$$\Delta\sigma_f(x) = \frac{4V_f\tau_s\left(L_f x - x^2\right)}{D_f L_f} \quad \dots \text{for SAF} \tag{102}$$

$$\Delta\sigma_f(x) = \frac{4V_f\tau_s\left(L_f x - x^2\right)}{3D_f L_f} \quad \dots \text{for SRF} \tag{103}$$

In the last two equations τ_s is equal to τ_0 if $w < w^*$, otherwise $\tau_s = \tau_s(w)$.

To summarize, the nominal stress in given Gauss point is computed as

$$\sigma_{NL} = \max\left(\sigma_{f,0} - \Delta\sigma_f\right)\cos(\phi) \tag{104}$$

The implemented algorithm in OOFEM is described in a schematic picture in Figure 11. The element in the center of the red circle contains crack(s) in its integration points and is a source of the fiber stress which is evaluated in its surrounding elements whose centers fall

- within the red circle with diameter a evaluated from (98) **and**
- within the blue band given by the projection of the source element in direction of the fiber orientation vector (CAF, SAF) or in direction of the crack normal (SRF). (In the individual integration points the normal vector can be different.)

Next, the fiber stress is computed from equation (104). The fiber bridging stress $\sigma_{b,f}$ in the source element and the reduction caused by snubbing $(\sigma_{b,f} - \sigma_{f,0})$ (99), (100) can be different in all integration points in that element. The distance x, used for evaluation of the fiber stress reduction $\Delta\sigma_f$ (101)–(103) caused by the interfacial bond stress, is computed from the coordinates of elements' centers. This is done for all integration points of the source element and the result is the maximum value.

A natural question arises what happens with the fiber stress in uncracked region if the crack undergoes unloading. When the crack is loaded, the fiber bridging stress is equilibrated by the resultant of shear stress τ as shown in Figure 12. The distribution of this stress and the debonded length a depends on the fiber class (CAF, SAF, SRF) and on the magnitude of the bond stress τ. During unloading the bridging stress in fibers decreases until it completely vanishes; during this phase the stretched fiber is being partially pulled back into the matrix. This reversed displacement gives rise to the bond stresses acting in the opposite direction than before. The resultant of the bond stresses must be in equilibrium. If the bond stress developing after unloading is of the same magnitude as the stress acting during loading, one half of the fiber (a/2) will be pulled away from the crack and the other half will be dragged into the crack and the stress distribution on the farther end of the fiber will remain unaffected. The largest "prestress" would be in the distance $a/2$ from the crack, see Figure 12. However, larger magnitude of the reversed bond stress would shift the position of

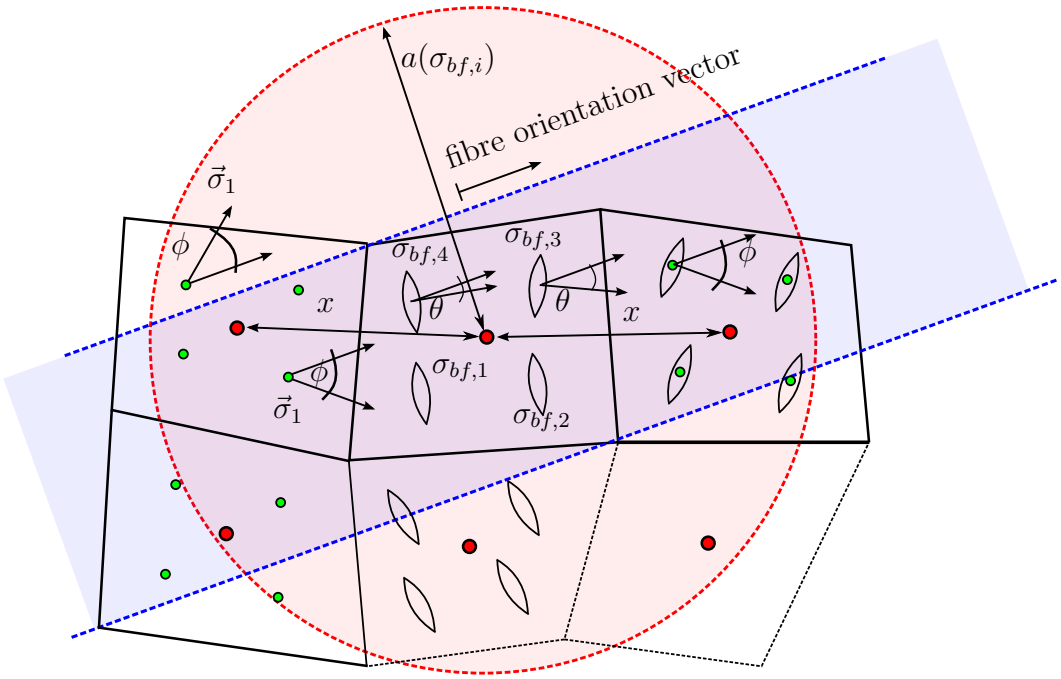

Figure 11: Evaluation of the stress in fibers in the vicinity of an element containing a crack. The stress in nonzero only in elements which fall into the circle with radius a (shown in red) and are in the band (shown in blue) defined by the projection of the element in the direction of the fiber orientation vector (CAF and SAF fibers) or the crack orientation (SRF fibers).

the maximum prestress towards the crack as indicated by the dotted line. Since the magnitude of this bond stress is questionable (the pulled out fiber can be bent over the crack face or its face can be scratched) and therefore the position of the peak of the prestress is uncertain, the fiber stress in the uncracked region is for simplicity idealized as never decreasing, it can only grow.

Distribution of the fiber bridging and nonlocal stresses evaluated according to equations (99)–(104) is shown in Fig. 13. The horizontal axis in this figure is in the case of the inclined aligned fibers not the normal direction to the crack surface, it is the distance measured along the fibers; similarly, the (nominal) nonlocal stress is not evaluated in the normal direction but in direction of the fibers. This figure nicely shows that the length of the debonded zone is indeed the same for different fiber orientations, alignment and length. It is also interesting

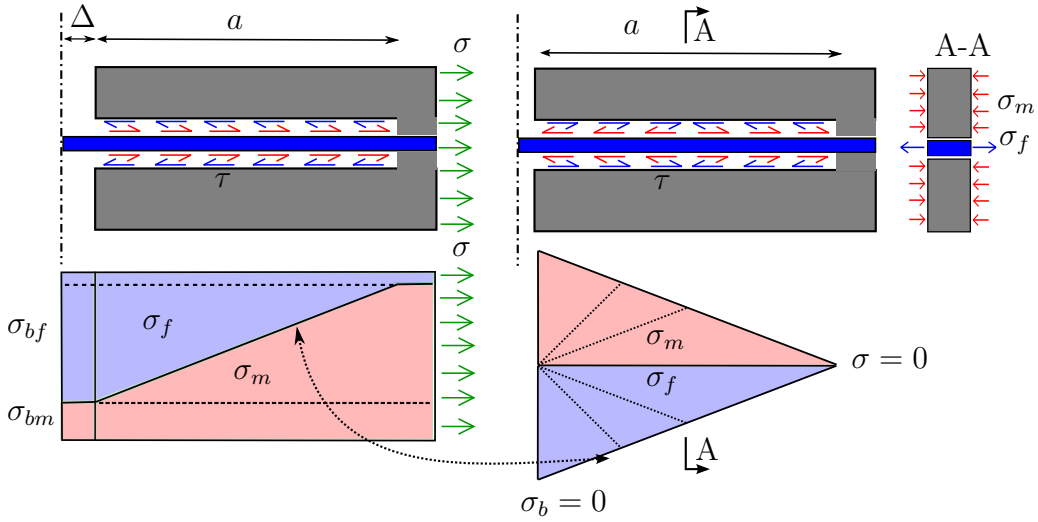

Figure 12: Distribution of nominal stresses in the matrix and fibers near the loaded (left) and unloaded (middle) crack. The middle figures demonstrate that even after unloading the material is not stress-free, the matrix is in compression and the fibers transfer tension, as shown in the right picture.

to examine the difference between the fiber bridging stress (shown for $x < 0$ and the nonlocal stress just behind the crack surface, $\sigma_{f,0}$. At constant angle θ (the angle between crack normal and the fiber orientation vector) the difference between these two stresses increases with increasing snubbing coefficient f. On the other hand, at large angle θ the bridging stress can be smaller than the nonlocal stress; the reason for this follows from the number of fibers crossing the crack which is very small for large θ which in turn leads to a small value of nominal stress. On contrary, in the direction of fibers, the volume fraction remains the same and is equal to V_f. The curves in Fig. 13 were obtained with $E_f = E_m = 20$ GPa, $V_f = 0.02$, $D_f = 40$ μm, $L_f = 12$ mm, $\tau_0 = 0.5$ MPa, $f = 0.5$, and crack opening 1 μm, 10 μm and 30 μm.

7.3 Crack initiation

In the nonlocal model the crack becomes initiated once the highest positive stress in matrix exceeds its tensile strength f_t. The effective stress in the matrix is computed as a difference of the investigated normal stress and the nonlocal

stress in the same direction divided by the volume fraction of matrix,

$$\bar{\sigma}_m = \frac{\sigma - \sigma_{NL}}{1 - V_f} \tag{105}$$

The material parameters are summarized in Tables 1 (matrix), 2 (fiber extension), and 3 (nonlocal extension).

Description	Nonlocal fixed crack model for FRC
Record Format	**FRCFCMNL** input record of ConcreteFCM and FRCFCM $r_{(rn)}$ # $wft_{(in)}$ #
Parameters	- r nonlocal radius (reasonable value is several millimeters and its maximum is $L_f/2$ for short fibers) - *wft* nonlocal averaging function, must be set to 4 (constant function)
Supported modes	PlaneStress

Table 3: Nonlocal fixed crack model for fiber reinforced concrete – summary.

The following the material definition can be treated as an example of SHCC material with volume density 24 kN/m^3, thermal dilation coefficient 12×10^{-6} K^{-1}, **properties of the matrix**: Young's modulus 20 GPa, Poisson's ratio 0.2, fracture energy 5 N/m, tensile strength 2 MPa, exponential softening, constant shear retention factor $\beta = 0.01$, unlimited shear strength (`shearStrengthType = 0`), **properties of the fibers**: short random fibers, volume fraction $V_f = 2\%$, diameter $D_f = 0.04$ mm, length $L_f = 12$ mm, Young's modulus of $E_f = 20$ GPa, shear modulus $G_f = 1$ GPa, fiber-matrix bond strength $\tau_0 = 0.5$ MPa, snubbing coefficient $f = 0.5$, shear correction coefficient $k = 0.9$, deactivated fiber damage, fiber act if COD exceeds 1 μm (with smoothing from $w = 0.9$ to 1.1 μm); the analysis uses [m], [MPa] and [MN]:

```
FRCFCMNL 1 d 24.e-3 talpha 12.e-6 E 20000. n 0.2 Gf 5.e-6 ft 2.0
softType 2 shearType 1 beta 0.01 FiberType 2 Vf 0.02 Df 0.04e-3
Lf 12.e-3 Ef 20000. Gfib 1000. tau_0 0.5 FSStype 0 f 0.5 kfib 0.9
fDamType 0 fibreactivationopening 1.e-6 dw0 1.e-7 dw1 1.e-7 r 6.e-3
wft 4
```

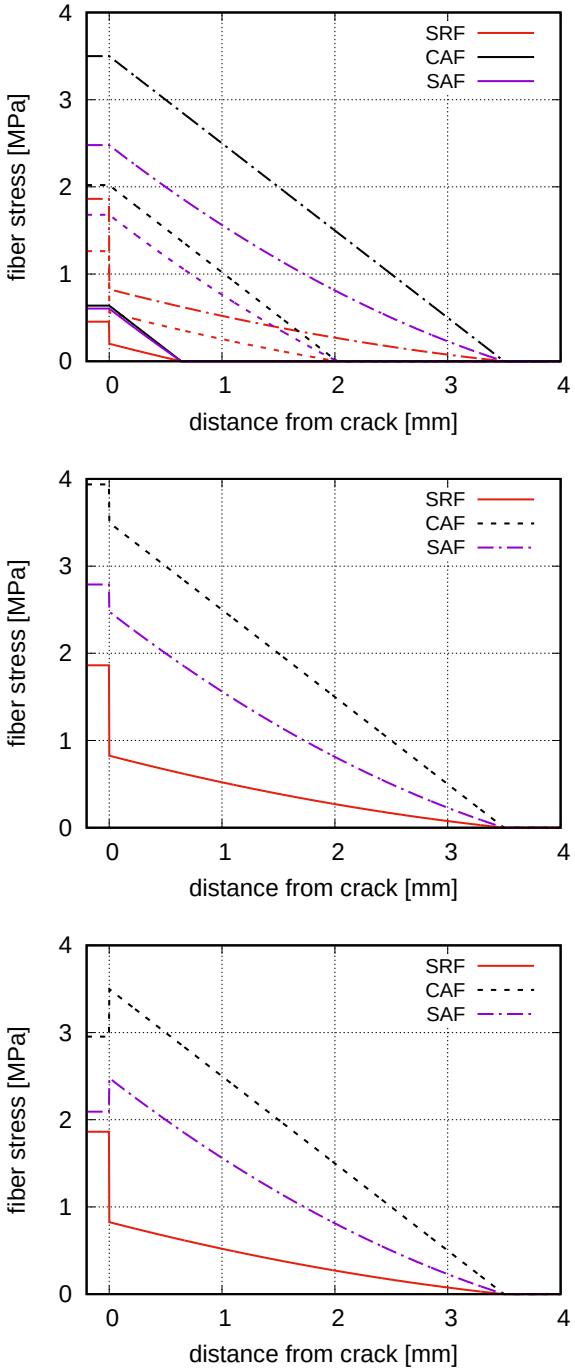

Figure 13: Fiber bridging stress (for $x < 0$) and the fiber nonlocal stress for CAF, SAF and SRF and $\theta = 0$ (top), $\theta = 30°$ (middle), and $\theta = 60°$ (bottom).

8 Tests

This section describes a collection of tests performed on a single finite element. These tests serve to verify that the numerical results correspond to the analytical or expected solution as well as to easily check that the changes in the finite element code performed by the other developers and contributors do not interfere with this material model. The first and the second set of tests examine the behavior in uniaxial loading of `ConcreteFCM` and `FRCFCM` material models while the third and the fourth set investigate the shear with the interaction of preexisting cracks.

There are two packages of test files which give exactly the same results. The first condensed (the detailed tests performed on a single finite element are merged in a single file to run more efficiently) package is in the OOFEM tests/sm folder and in those tests the errorcheck mode is activated. If the computed value does not match the defined value an error message is produced. The second group of tests is here in the documentation folder. When the file is run in OOFEM, postprocessed with extractor.py, then the corresponding *.gnu file will give the graphical output (in postscript); such outputs are presented hereafter.

In the subsequent figures the lines usually correspond to the analytical solution and the black points to the numerical. The crack width is evaluated from the computed results as $w = (\varepsilon - \sigma/E)h$ where the member in the parentheses is equal to the cracking strain ε_{cr}.

The material parameters are specified in compatible units with m and MN.

8.1 ConcreteFCM in tension

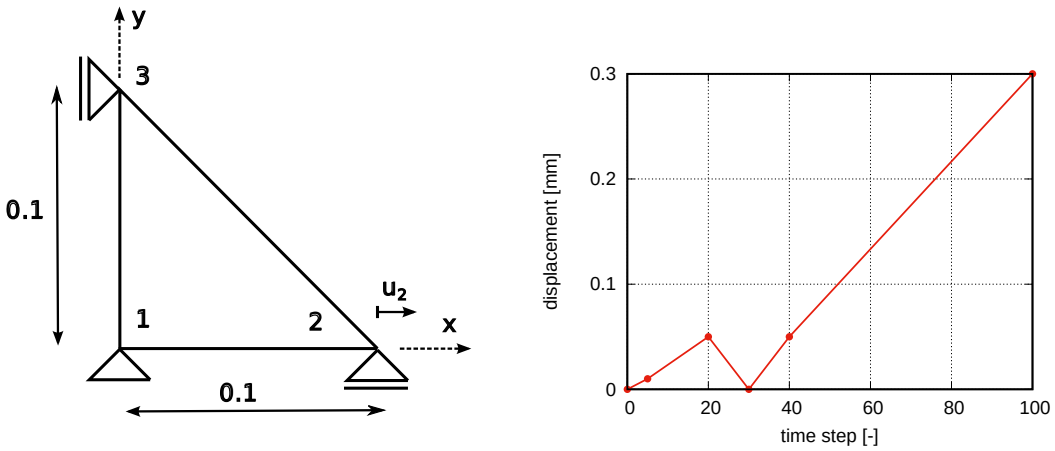

Figure 14: Geometry (left) and the loading program (right) for the tensile tests. The analysis runs in plane stress under a direct displacement control. The elastic properties are $E = 20$ GPa and $\nu = 0.2$.

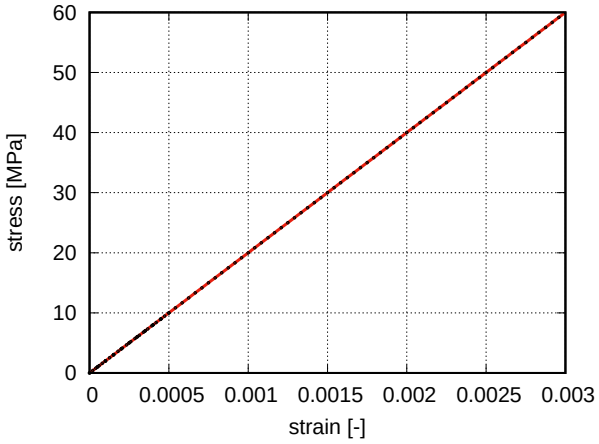

Figure 15: Test `concrete_fcm_st_0`, geometry and loading according to Fig. 14, the material behaves as linear elastic (`softType 0`).

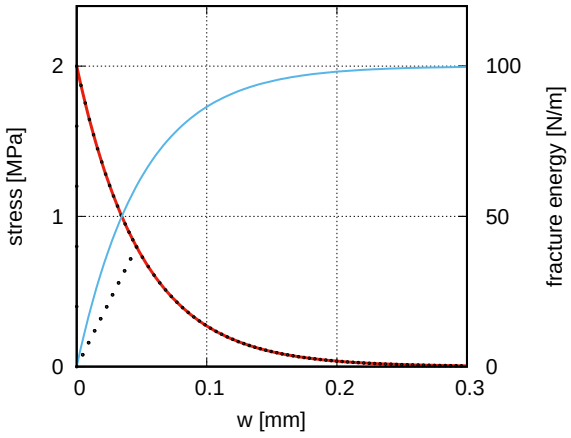

Figure 16: Test `concrete_fcm_st_1`, geometry and loading according to Fig. 14, the postpeak behavior is with **exponential** softening (`softType 1`), $f_t = 2$ MPa and $G_f = 100$ N/m .

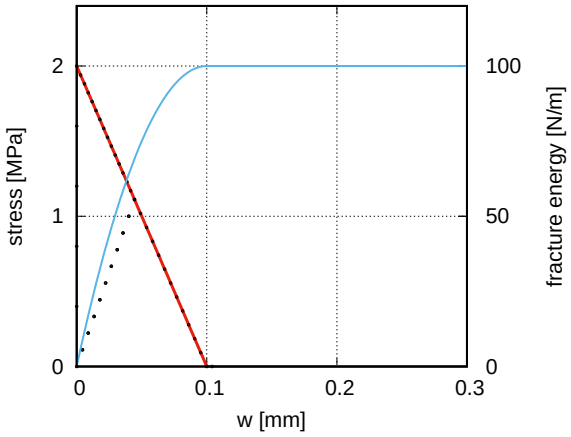

Figure 17: Test `concrete_fcm_st_2`, geometry and loading according to Fig. 14, the postpeak behavior is with **linear** softening (`softType 2`), $f_t = 2$ MPa and $G_f = 100$ N/m .

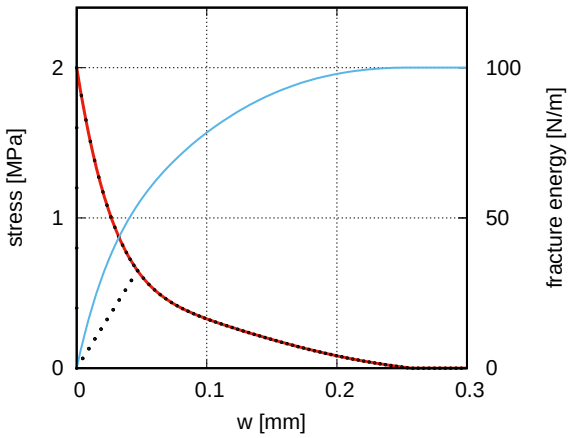

Figure 18: Test `concrete_fcm_st_3`, geometry and loading according to Fig. 14, the postpeak behavior is with softening according to **Hordijk** (`softType 3`), $f_t = 2$ MPa and $G_f = 100$ N/m .

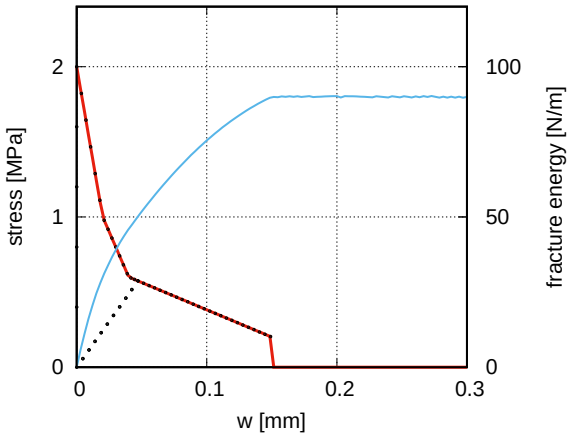

Figure 19: Test `concrete_fcm_st_4`, geometry and loading according to Fig. 14, the postpeak behavior is user-defined (`softType 4`), $f_t = 2$ MPa, `soft_w 4 0. 2.e-5 4.e-5 15.e-5 soft(w) 4 1. 0.5 0.3 0.1`.

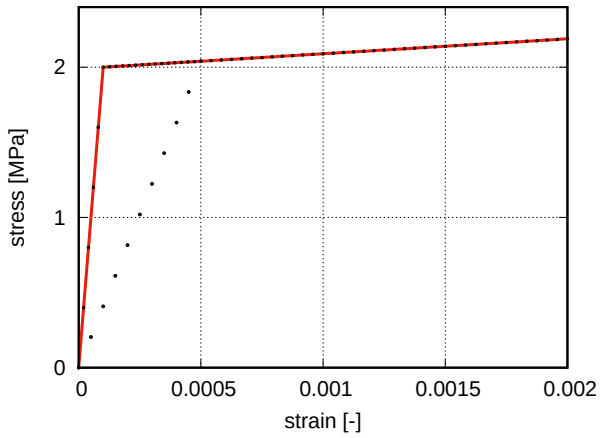

Figure 20: Test `concrete_fcm_st_5`, geometry and loading according to Fig. 14, the postpeak behavior is with linear hardening (`softType 5`), $f_t = 2$ MPa, `H 100. eps_f 1.e-2`

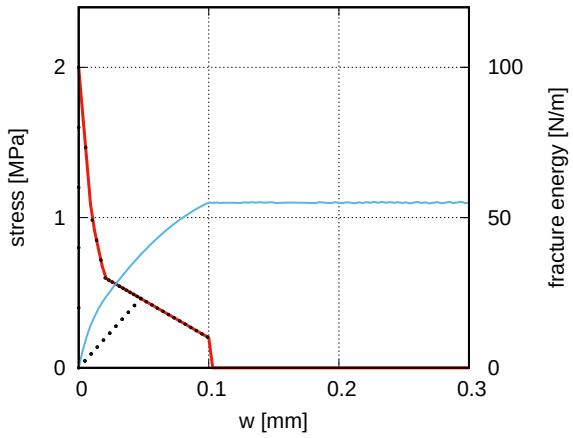

Figure 21: Test `concrete_fcm_st_6`, geometry and loading according to Fig. 14, the postpeak behavior is captured by user-defined strain-dependent behavior (`softType 6`), $f_t = 2$ MPa, `soft_eps 4 0. 1e-4 2e-4 1e-3 soft(eps) 4 1. 0.5 0.3 0.1`

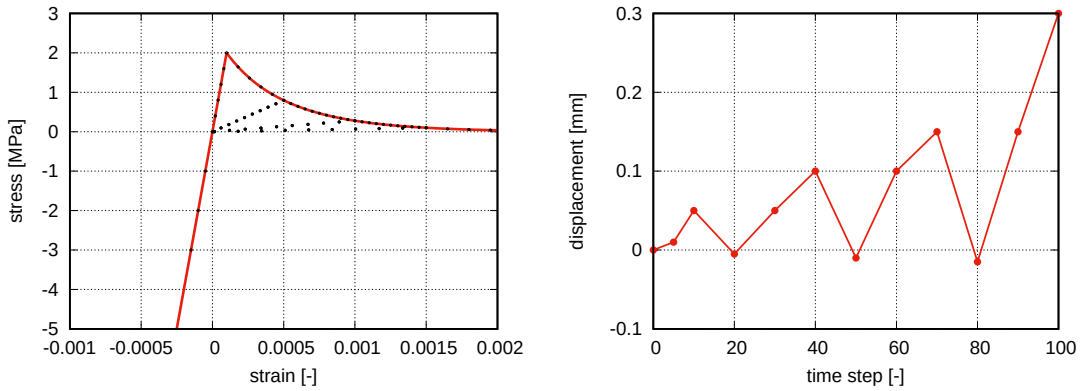

Figure 22: Test `concrete_fcm_unlo` and the associated loading; geometry is according to Fig. 14, the postpeak behavior is with exponential softening (`softType 1`), $f_t = 2$ MPa and $G_f = 100$ N/m .

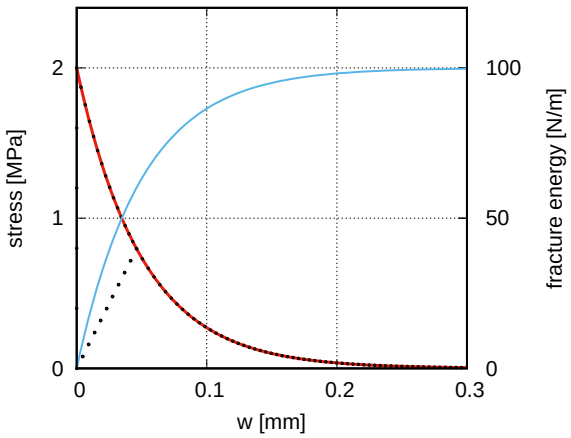

Figure 23: Test `concrete_fcm_crack_spacing`, geometry and loading from Fig. 14 is modified - the horizontal dimension and the magnitude of the prescribed displacement are doubled, the postpeak behavior is with exponential softening (`softType 2`), $f_t = 2$ MPa and $G_f = 100$ N/m .

8.2 FRCFCM in tension

If not stated otherwise, the matrix in the following examples is characterized by following material properties: $E = 20$ GPa, $\nu = 0.2$, $f_t = 2$ MPa, $G_f = 100$ N/m, linear softening (`softType 2`). The fiber content is V_f, diameter $D_f = 40$ μm, elastic modulus $E_f = 20$ GPa, shear modulus $G_{fib} = 1$ GPa, strength of bond between fiber and matrix $\tau_0 = 1$ MPa, snubbing coefficient $f = 0.7$, fiber cross-section correction factor $k = 0.9$ (`Vf 0.02 Df 0.04e-3 Ef 20000. Gfib 1000. tau_0 1. f 0.7 kfib 0.9`). The default value for the exponent M (unloading-reloading) is 4. With one exception, all verification tests use the geometry defined in Fig. 14.

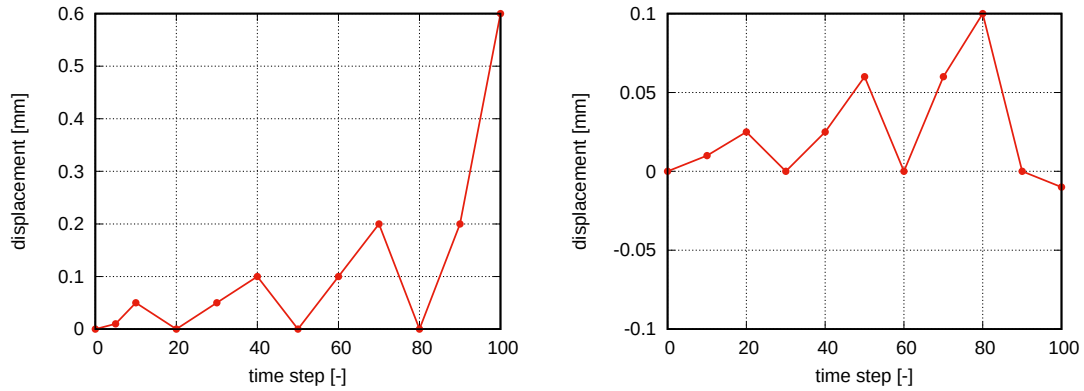

Figure 24: Loading program for the tensile tests of the fiber-reinforced material.

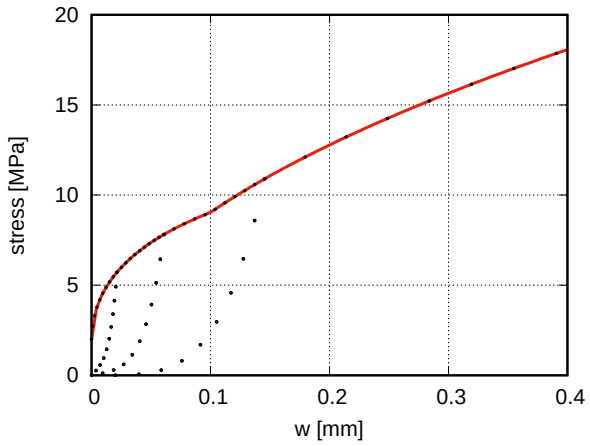

Figure 25: Test `frcfcm_1_CAF`, loading described in Fig. 24a; continuous aligned fibers (`FiberType 0`), fibers are oriented in direction of x-axis (default option).

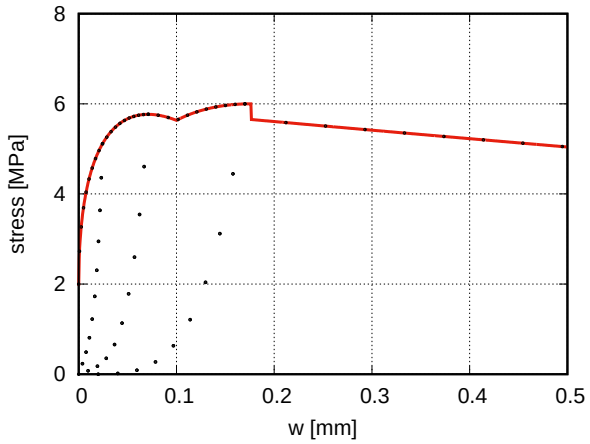

Figure 26: Test `frcfcm_2_SAF`, loading described in Fig. 24a; short aligned fibers (`FiberType 1`), fibers are oriented in direction of x-axis (default option).

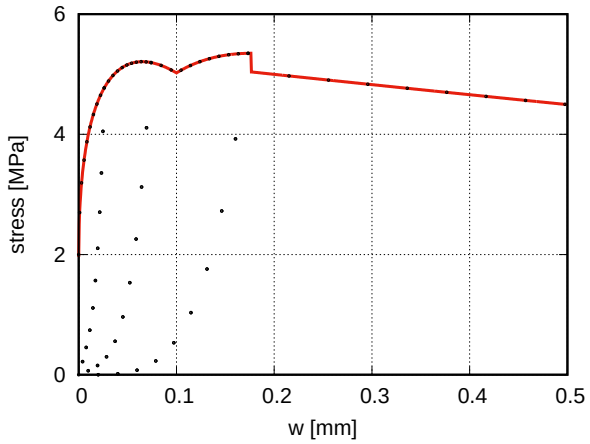

Figure 27: Test `frcfcm_3_SRF`, loading described in Fig. 24a; short random fibers (`FiberType 2.`)

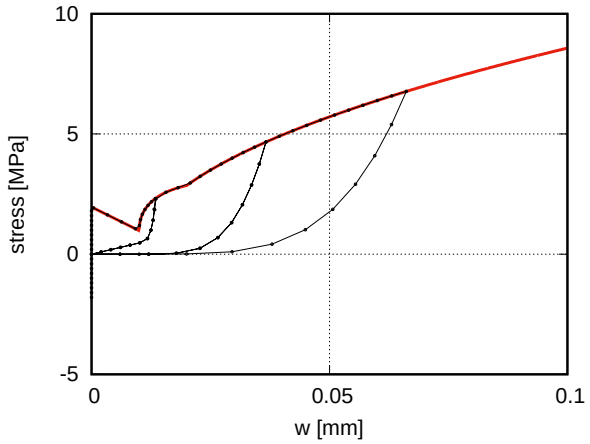

Figure 28: Test `frcfcm_4_CAF_activation_opening`, loading is defined in Fig. 24b; continuous aligned fibers, fiber activation opening 10 μm (`fibreActivationOpening 10.e-6`).

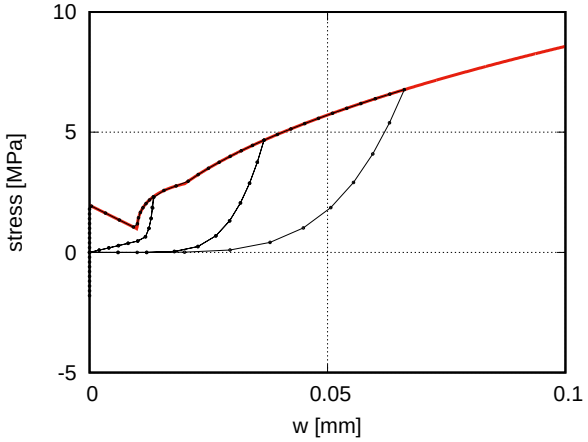

Figure 29: Test `frcfcm_5_CAF_crack_spacing`, geometry and loading from Fig. 14 and Fig. 24b is modified: the horizontal dimension and the magnitude of the prescribed displacement are doubled; continuous aligned fibers, fiber activation opening 10 μm (`fibreActivationOpening 10.e-6`), crack spacing 0.1 m (`crackSpacing 0.1`).

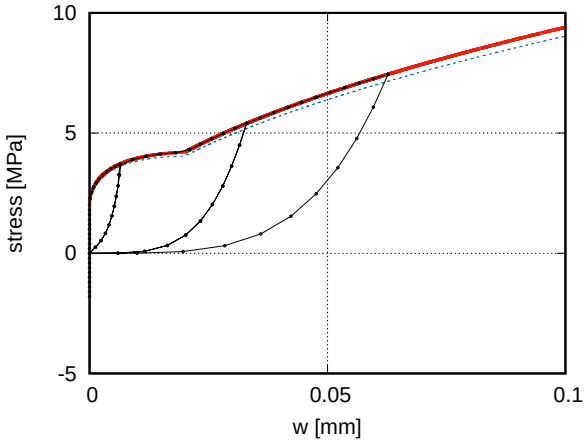

Figure 30: Test `frcfcm_6_CAF_fibre_orientation_snubbing`, loading is defined in Fig. 24b; continuous aligned fibers, fibre orientation at 60° `fibreOrientationVector 3 0.5 0.866025403784439 0.`; the thin blue line shows the reference case when all fibers are horizontal (the snubbing does not apply and the fiber quantity is higher).

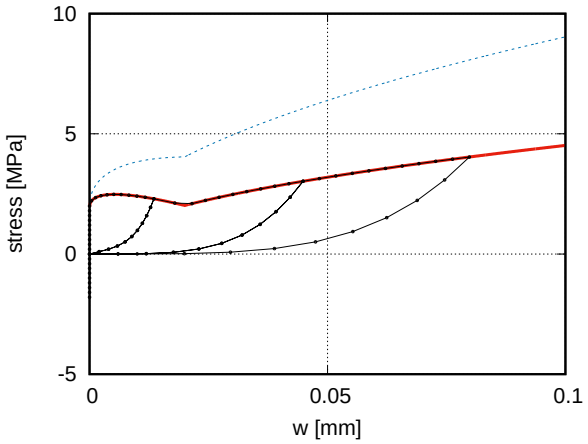

Figure 31: Test `frcfcm_7_CAF_fibre_orientation_no_snubbing`, loading is defined in Fig. 24b; continuous aligned fibers, snubbing coefficient $f = 0$ (`f 0.`), fibre orientation at 60° `fibreOrientationVector 3 0.5 0.866025403784439 0.`; the thin blue line shows the reference case when all fibers are horizontal (the snubbing does not apply and the fiber quantity is higher).

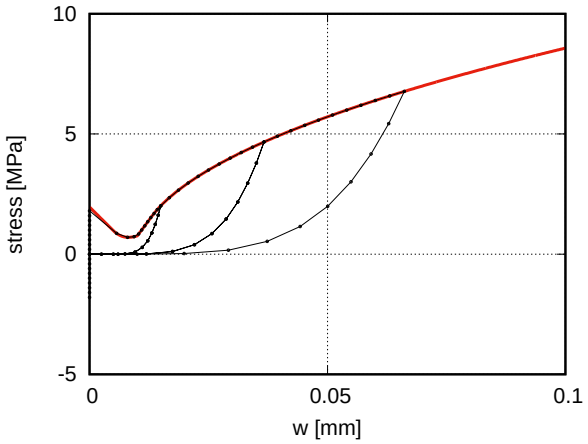

Figure 32: Test `frcfcm_8_CAF_activation_opening_smooth`, loading is defined in Fig. 24b; continuous aligned fibers, fiber activation opening 10 μm (`fibreActivationOpening 10.e-6`), smooth transition from 5 μm to 15 μm (`dw0 5.e-6 dw1 5.e-6`).

8.3 ConcreteFCM in shear

This Section describes tests which aim at verification of the shear stiffness and strength after the onset of cracking. These properties are tested on a single quadrilateral plane-stress finite element, shown in the left part of Figure 33. This element is subjected to uniform biaxial loading and shear which are defined via displacements u_2, u_3, u_4 and v_3 and v_4. The loading is divided into several intervals. First, the element is stretched in the x-direction ($u_3 = v_3 = v_4 = 0$ and $u_2 = u_4$) causing first crack to appear. This deformation is then kept constant throughout the rest of the analysis. Second, the shear deformation is increased and then returned back to zero ($u_3 = u_4$ and $v_3 = v_4 = 0$). Next, the element is stretched in the vertical direction ($v_3 = v_4$) and consequently is subjected to another shear cycle. The loading program is shown in the right part of Figure 33.

The elastic properties are $E = 20$ GPa and $\nu = 0.2$, the tensile strength $f_t = 2$ MPa, fracture energy $G_f = 100$ N/m, softening is linear (`softType 2`).

The geometry is the same in all tests. The loading is preserved in all simulations except for the tests on the shear strength where the magnitude of the shear deformation cycles is increased.

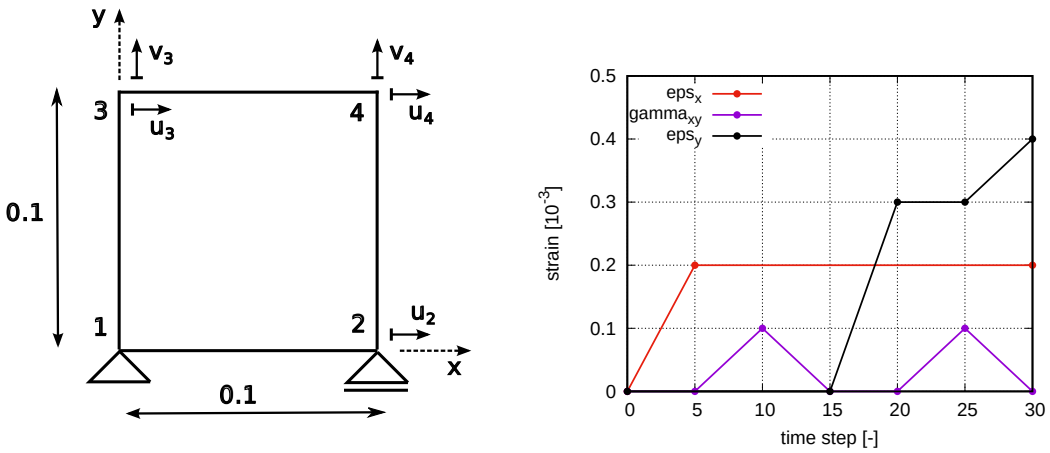

Figure 33: Geometry (left) and the loading program (right) for the shear tests. The analysis runs in plane stress under a direct displacement control.

The output with a brief description is presented in the following figures. The solid line usually corresponds to the analytical solution while the black points

to the computed values. In most cases the test was is performed two times with a subtle modification: either the shear stiffness is evaluated from the dominant (wider crack) or from both cracks (`multipleCrackShear` keyword).

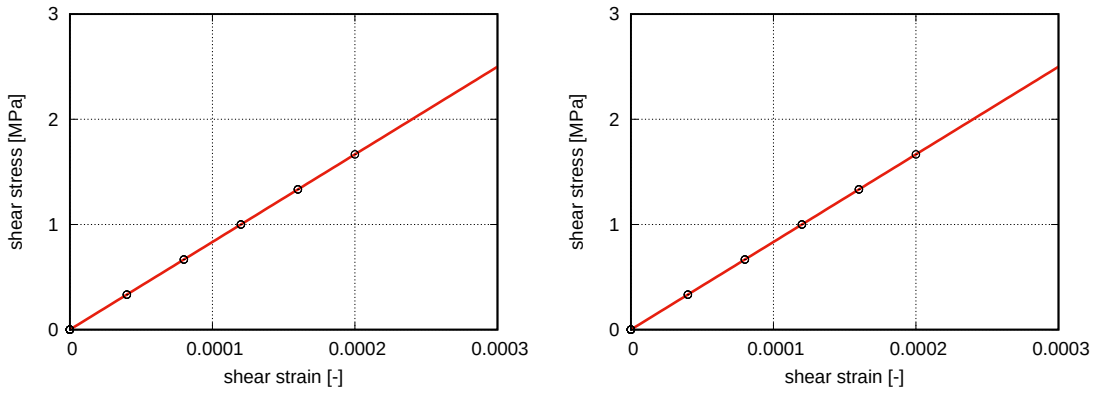

(a) (b)

Figure 34: Computed shear stress vs. shear strain for case when tensile cracking does not lead to any decrease in shear stiffness (`shearType 0`); a = dominant crack response, b = multiple cracks. Test files are labeled `concrete_fcm_shear_none` + `dominant/multiple`.

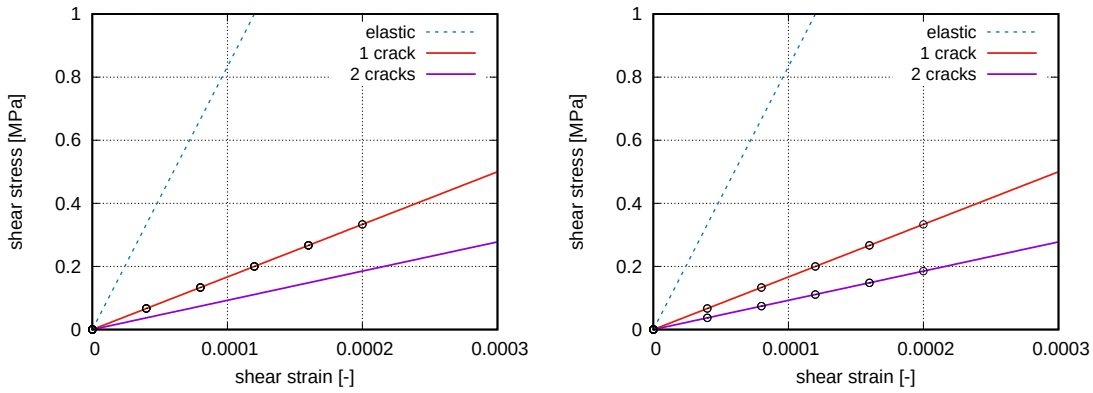

(a) (b)

Figure 35: Computed shear stress vs. shear strain for case when cracking leads to a constant decrease in shear stiffness controlled by the shear retention factor $\beta = 0.2$ (`beta 0.2`) activated by keyword (`shearType 1`); a = dominant crack response, b = multiple cracks. Test files are labeled `concrete_fcm_shear_beta` + `dominant/multiple`.

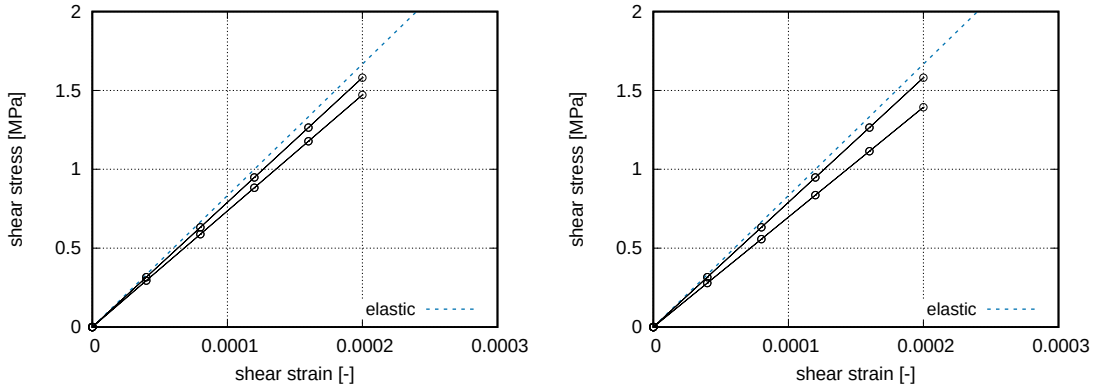

(a) (b)

Figure 36: Computed shear stress vs. shear strain for case when cracking leads to a variable decrease in shear stiffness controlled by the shear factor coefficient $s_F = 10$ (`sf 10.`) activated by keyword (`shearType 2`); a = dominant crack response, b = multiple cracks. Test files are labeled `concrete_fcm_shear_sf` + `dominant/multiple`.

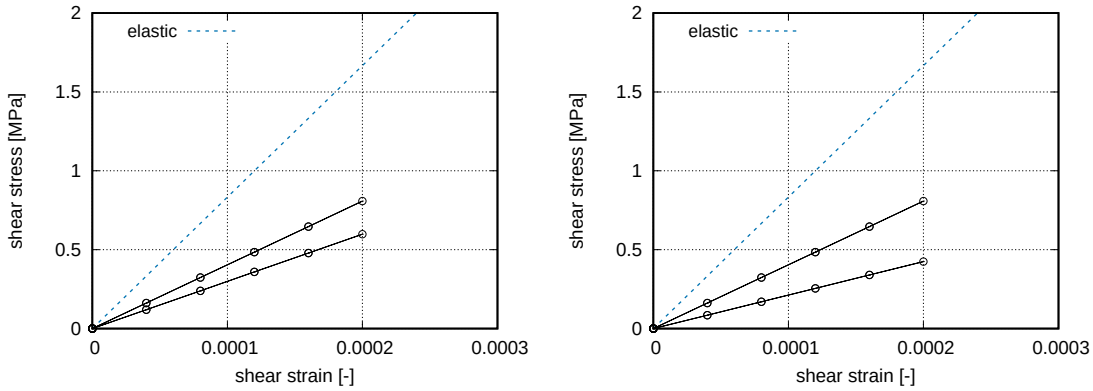

Figure 37: Computed shear stress vs. shear strain computed when cracking leads to a user-defined decrease in shear stiffness controlled by variable shear retention factor $\beta(w)$ (`beta_w 6 0. 1.e-6 5.e-6 1.e-5 5.e-5 1.e-3 beta(w) 6 1. 1. 0.5 0.5 0.1 0.1`) activated by keyword (`shearType 3`); a = dominant crack response, b = multiple cracks. Test files are labeled `concrete_fcm_shear_userbeta` + `dominant/multiple`.

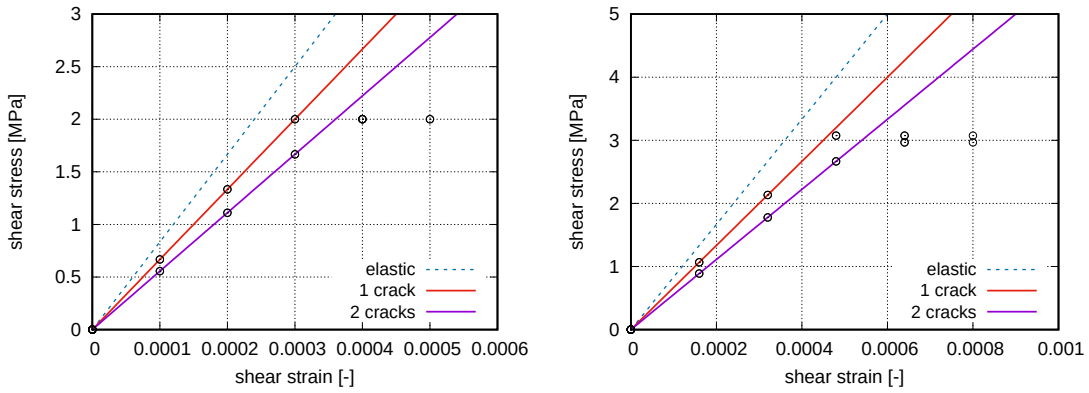

(a) (b)

Figure 38: Computed shear stress vs. shear strain for case when the shear strength is limited, shear stiffness is reduced by a constant shear retention factor $\beta = 0.8$ (`beta 0.8`), multiple cracks contribute to the overall shear stiffness, and shear strain loading is more pronounced than in the previous cases; (a): shear strength limited by the tensile strength f_t (`shearStrengthType 1`), (b): shear strength follows the formula proposed by Collins (41), (`shearstrengthtype 2 fc 30 ag 0.01 lengthscale 1.` Test files is labeled `concrete_fcm_shear_strength`.)

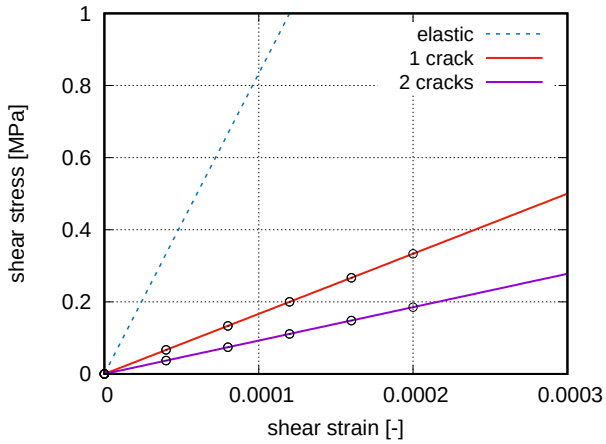

Figure 39: Computed shear stress vs. shear strain for case when cracking leads to a constant decrease in shear stiffness controlled by the shear retention factor $\beta = 0.5$ (`beta 0.5`), more cracks contribute to the shear stiffness, and parallel cracks with crack spacing 0.025 m develop (`crackSpacing 0.025`). Test files are labeled `concrete_fcm_shear_crack_spacing` + `dominant/multiple`.

8.4 FRCFCM in shear

This section shows the results of three verifying shear tests carried out on a single finite element with a material model FRCFCM. The loading and geometry are the same as described in the previous section.

The elastic properties of the **matrix** are $E = 20$ GPa and $\nu = 0.2$, the tensile strength $f_t = 2$ MPa, fracture energy $G_f = 100$ N/m, softening is linear (`softType 2`), shear stiffness is reduced by a constant shear retention factor $\beta = 0.01$, and the shear stiffness is affected by multiple cracking. In all three cases the volume fraction of fibers is $V_f = 0.02$, fiber diameter $D_f = 40$ μm, elastic (axial) stiffness $E_f = 20$ GPa, elastic shear stiffness $G_f = 1$ GPa, bond strength between the fiber and matrix $\tau_0 = 1$ MPa (constant), snubbing coefficient $f = 0.7$, and fiber shear correction factor $k_{fib} = 0.9$; in OOFEM syntax (fibers only): `Vf 0.02 Df 0.04e-3 Ef 20000. Gfib 1000. tau_0 1. f 0.7 kfib 0.9 FSStype 0.`

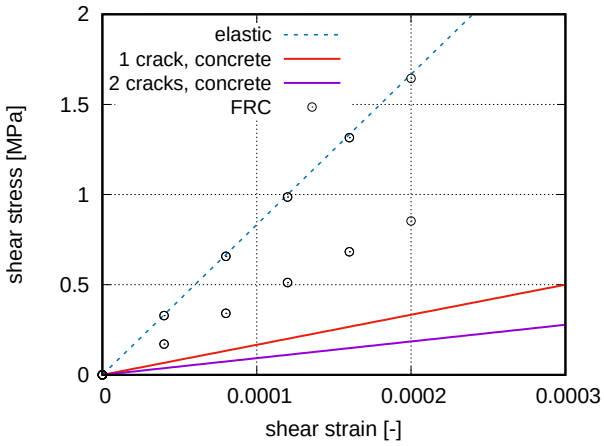

Figure 40: Computed shear stress vs. shear strain for CAF with orientation vector $x : y : z = 10 : 1 : 0$ (`FiberType 0 fibreOrientationVector 3 10. 1. 0.`). Test file is labeled `frcfcm_shear_CAF_beta_multiple`.

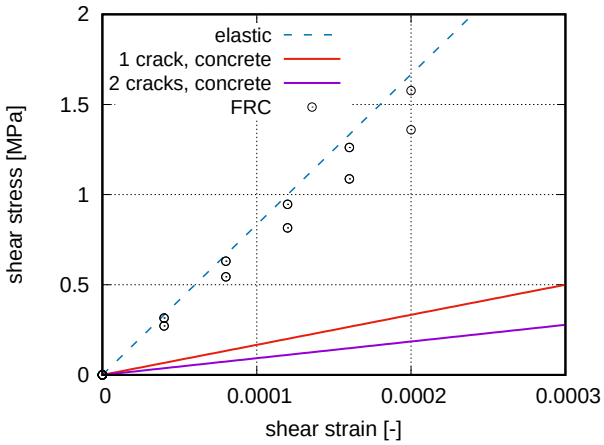

Figure 41: Computed between shear stress and shear strain for SRF and predefined crack spacing 25 mm (`FiberType 2 crackSpacing 0.025`). Test file is labeled `frcfcm_shear_SRF_beta_multiple.`

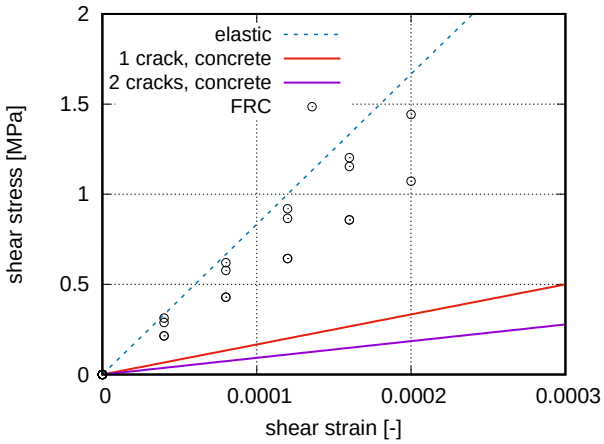

Figure 42: Computed relationship between shear stress and shear strain for SRF, predefined crack spacing 25 mm and exponential fiber damage with $\gamma_{crack} = 0.5$ (`FiberType 2 crackSpacing 0.025 fDamType 2 gammaCrack 0.5`). Test file is labeled `frcfcm_shear_SRF_beta_multiple_damage.`

9 Benchmark

This section demonstrates the capabilities of the nonlocal variant of the FR-CFCM model. The nonlocal model is computationally very expensive and requires many iterations to reach an equilibrium. For this reason the benchmark problem was chosen as simple as possible to show the prevailing trends in a limited time. To illustrate the importance of the nonlocal concept, the results obtained with the local version of the model are presented first.

The geometry of the computational model is shown in Figure 43. The length is $L_x = 25$ mm and the maximum width $b_{max} = 2$ mm. The width is not uniform, the thinnest cross-section is in the midspan where the width is reduced to 1.5 mm. The function describing the width $b(x)$ is a second-order parabola. The specimen is symmetric about both its vertical and horizontal axes.

The computational model is composed by one row of uniformly spaced plane-stress quadrilateral elements. To test the objectivity of the material model, the finite element mesh has been generated with three different densities (but still with one element per width). The model named as coarse is composed of 21 elements, model medium 41, and the finest mesh comprises 81 elements.

The loading of the model is defined by either direct load or direct displacement control. The loading is applied at the rightmost two nodes while the (two) pinned supports are at the left end.

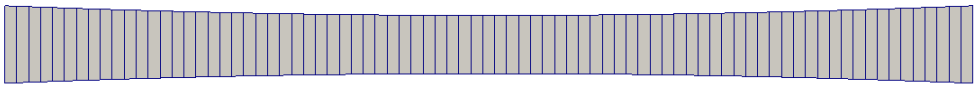

Figure 43: Finite element mesh for uniaxial tension problem (fine mesh with 81 elements).

The material model corresponds to a strain hardening cementitious material with 2% per volume of either continuous aligned or short (12 mm long) random fibers. The fibers are embedded in a very brittle matrix with $G_f = 5$ N/m and $f_t = 2$ MPa, the type of softening is exponential. The linear unloading of fibers (to Δw) leads to improved convergence, for this reason it is used here instead of 4° parabola. A detailed syntax of the nonlocal model with CAF

fibers the material syntax is `frcfcmnl 1 d 0. talpha 0. E 20000. n 0.2 Gf 5.e-6 ft 2.0 softtype 1 sheartype 1 beta 0.01 Vf 0.02 Df 40.e-6 Lf 12.e-3 Ef 20000. Gfib 1000. tau_0 0.5 f 0.5 kfib 0.9 FSStype 0 fDamType 0 FiberType 0 ncracks 1 fibreActivationOpening 1.e-6 r 0.02 wft 4 dw0 1.e-7 dw1 1.e-7 M 1 fibreOrientationVector 2 1. 0.`

The following table gives the idea of the computational cost (Intel i5 at 2.3 GHz). The price for the computation is given partially by a high number of brittle crack openings and by a large number of loading steps which is necessary in order to generate the cracks one-by-one.

Path + file name	Computational time
SRF_local/coarse_F_local/neck.in	3 s
SRF_local/medium_F_local/neck.in	7 s
SRF_local/fine_F_local/neck.in	17 s
SRF_local/coarse_local_local/neck.in	1 m 2 s
SRF_nonlocal/coarse/neck.in	22 s
SRF_nonlocal/medium/neck.in	1 m 11 s
SRF_nonlocal/fine/neck.in	5 m 26 s
SRF_nonlocal/coarse_F/neck.in	6 s
CAF_nonlocal/coarse/neck.in	30 s
CAF_nonlocal/medium/neck.in	1 m 30 s
CAF_nonlocal/fine/neck.in	5 m 20 s

9.1 Local FRCFCM

The first crack is formed in the middle of the specimen (in the weakest element) when the normal stress exceeds the tensile strength. Under the direct displacement control, depending on the balance of the elastic energy accumulated in the specimen and the fracture energy of the matrix, the crack is opening either suddenly or slowly. As the crack is opening the rest of the specimen is unloading. If the traction-separation law is with hardening and the loading continues, the stress exceeds the tensile strength in the second weakest link this scenario is repeated until the whole specimen is saturated with cracks (CAF) or the traction-separation law starts softening in the crack with the widest opening (SAF or SRF).

The crack growth is for the coarse mesh and the local FRCFCM material model with short random fibers shown in Figure 44. The displacements in this figure are exaggerated. Interestingly, the difference in the crack opening is very

small, this is due to very fast growth of the fiber bridging stress once the crack opening exceeds Δw. The picture at the bottom is just before the state when the stress in the middle element exceeds the maximum stress of the material, $\sigma(w^*)$.

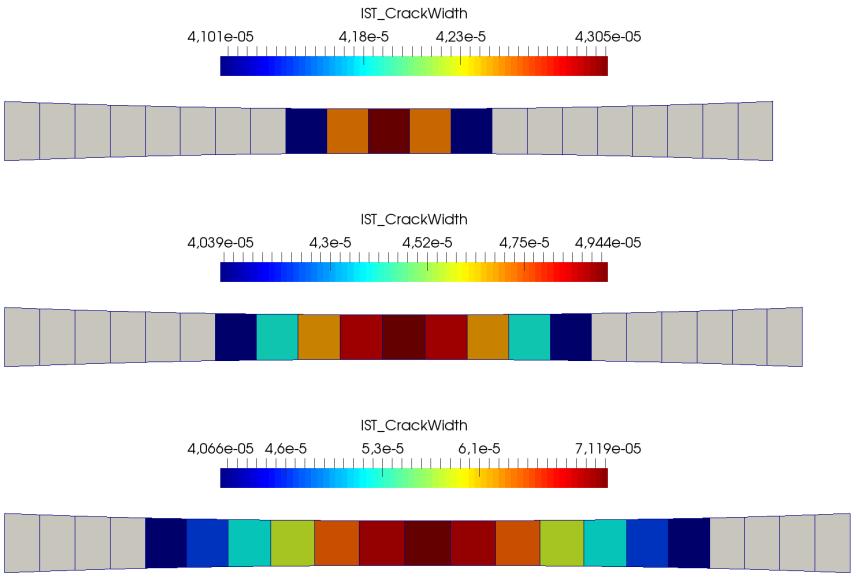

Figure 44: Computed crack widths displayed on a deformed **coarse** finite element mesh (the displacements are magnified and the scale is in meters); cracks start developing from the center and propagate towards the thicker sections of the model.

The load-displacement diagram in Figure 45 shows nice agreement of the displacement-driven and the force-driven analysis. Naturally, in the force-driven analysis one cannot get the sudden drops in force associated with brittle crack opening. It is worth mentioning that with more existing cracks these drops tends to decrease as the overall stiffness is substantially reduced. The height of these drops also depends on the exponent M in the unloading-reloading law but the influence is not significant. At the displacement ≈ 0.84 mm the crack opening in the weakest element reaches w^* and the force crack starts opening at decreasing stress.

However, if the mesh density was doubled (in the axial direction), the cracks would have been initiated in twice as much elements and the overall deformation would have increased (almost) twofold (because the elastic deformation is negligible compared to the cracking deformation). Crack propagation on $4\times$ finer

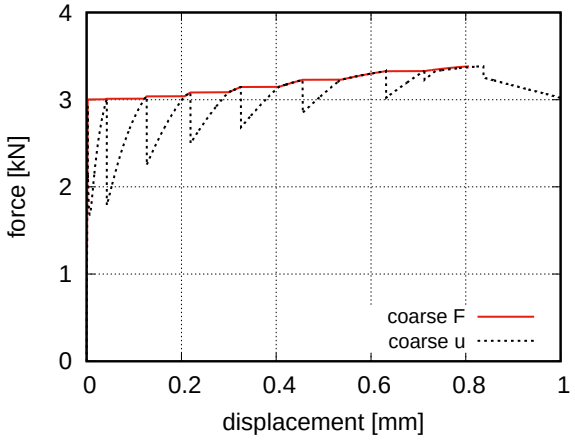

Figure 45: Load-displacement diagram obtained with the local FRCFCM model with short random fibers on a coarse mesh under direct displacement and force control.

mesh is shown in Figure 46 and the rate of the overall deformation growth in Figure 47. Naturally, such behavior is unacceptable. The local version of the FRCFCM material model must not be used for materials with hardening.

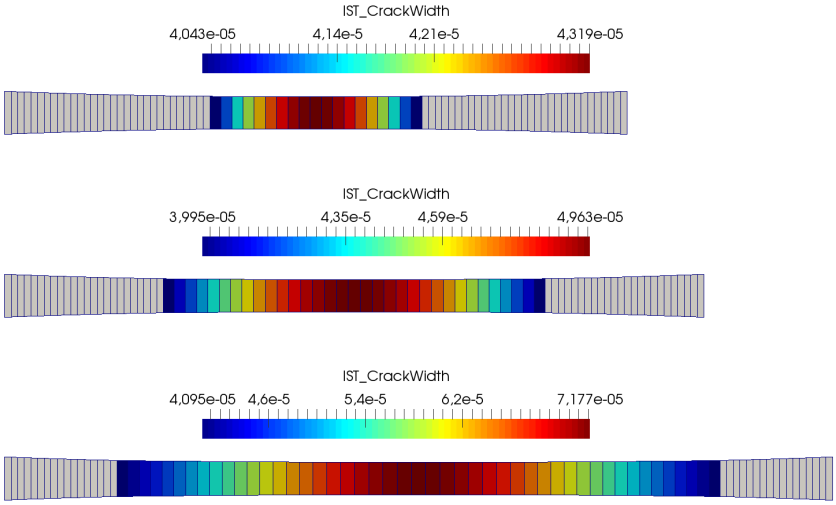

Figure 46: Computed crack widths displayed on a deformed **fine** finite element mesh (the displacements are magnified and the scale is in meters); cracks start developing from the center and propagate towards the thicker sections of the model. The individual time steps correspond to the three figures in Fig. 44; the crack openings as well as the length of the damaged zone are almost identical but the overall axial displacement is here four times higher.

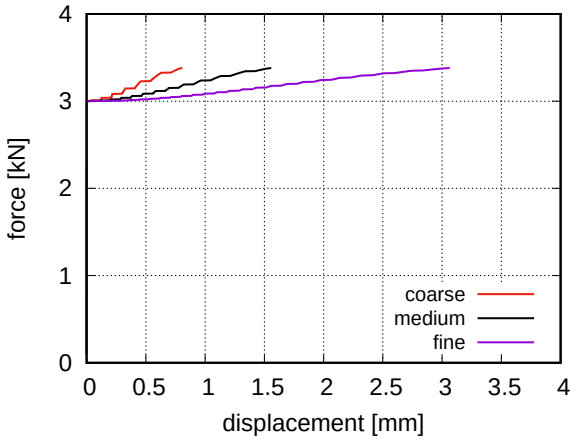

Figure 47: Load-displacement diagram obtained with the local FRCFCM models with short random fibers; analysis is run under direct force control. Due to the large displacements the elastic loading path is not apparent.

9.2 Nonlocal FRCFCM

The situation drastically changes if the local version of the FRCFM material model is replaced by its nonlocal extension. This is shown here for the **continuous aligned fibers**. After the formation of the first crack, the bridging stress in the fibers leads to a field of nonlocal fiber stress which decreases with the distance from the crack until it reaches zero for distance bigger than a (98), see the first figure in Figure 49 and 50. This nonlocal stress is then used in the condition for the formation of a subsequent crack (104). In this case, the stress-strength condition is not violated in the finite elements right next to the element with the first crack but in the second row. This is repeated until the cracks saturate the specimen and the load-displacement diagram is globally hardening without further kinks, see Figure 48. This diagram also indicates that the response is no longer dependent on the fineness of the finite element mesh; (almost) the identical curve is obtained for all three mesh densities (coarse, medium, fine) for loading displacement < 0.08 mm, afterwards some differences appear but the agreement is still good.

For the comparison of the crack distribution, their widths, and the nonlocal stress computed on a coarse and fine mesh, see Figures 49, 50, 51, and 52.

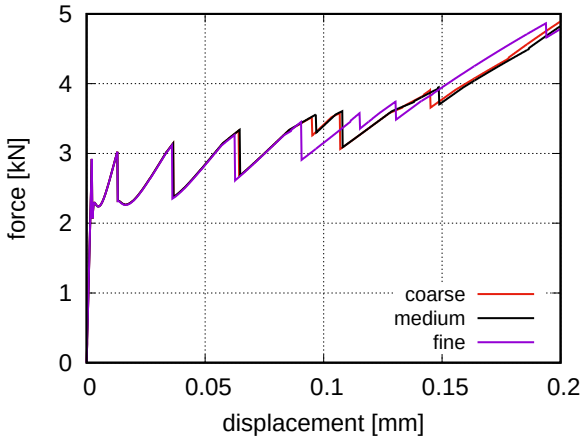

Figure 48: Load-displacement diagram obtained with the **nonlocal** FRCFCM models containing continuous aligned fibers; analysis was run under direct displacement control and was performed on three different finite element meshes.

In the case of the short random fibers only three cracks develop: the central and then one on each side. The distance between the cracks is bigger owing to

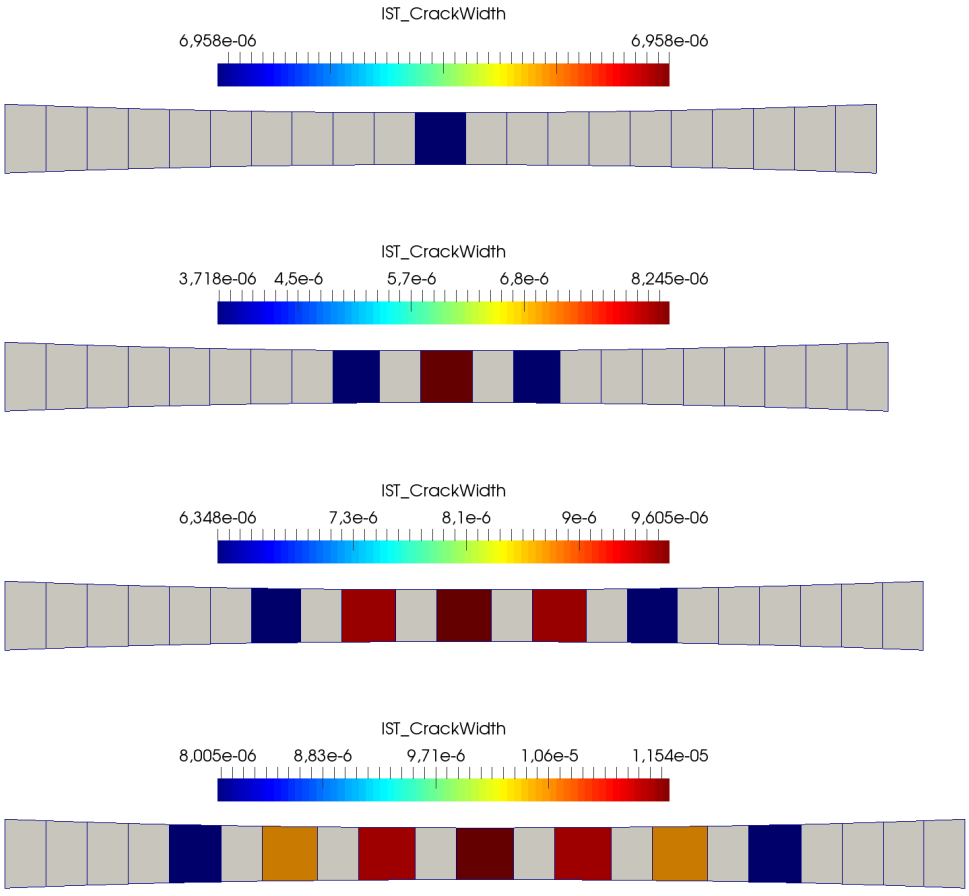

Figure 49: Computed crack widths displayed on a deformed **coarse** finite element mesh (the displacements are magnified and the scale is in meters); cracks start developing from the center and propagate towards the thicker sections of the model but the damaged elements do not neighbor. The distance is determined entirely by the material properties and the fiber class (in this case CAF).

a different stress transfer from fibers to matrix. The comparison of the global response is for the three mesh densities and direct displacement control and for the coarse mesh and direct force control shown in Figure 54. The crack distribution and the nonlocal stress is for the coarse mesh shown in Figure 49.

What is important and interesting is the comparison of the numerically computed crack-spacing with the values obtained using the analytically derived ex-

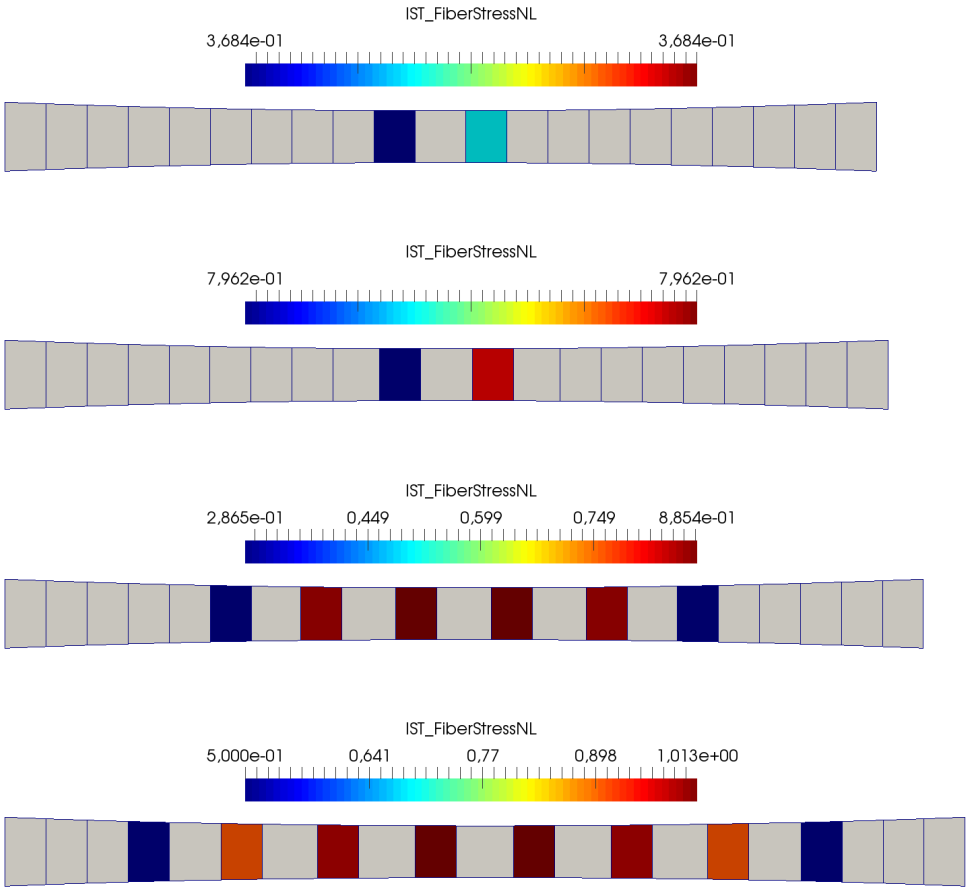

Figure 50: Nonlocal fiber stress in uncracked elements (expressed per unit are of the composite) displayed on a deformed **coarse** finite element mesh (the scale is in MPa); the time steps correspond to those from Fig. 49.

pressions presented earlier in equations (95)–(97). According to those formulas and the material definition of the benchmark problem, the crack spacing is for the continuous aligned fibers $x_{CAF} = 0.196$ mm and for the short random fibers $x_{SRF} = 3.83$ mm. In the numerical simulations these distances are $x_{CAF,OOFEM} = 2.16$ mm and $x_{SRF,OOFEM} = 4.32$ mm. (These distances were measured on the fine finite element mesh between the centers of the cracked elements.) It must be noted that the analytically derived expression hold for ideally brittle matrix. The error is around 10% and its source is the non-uniform width

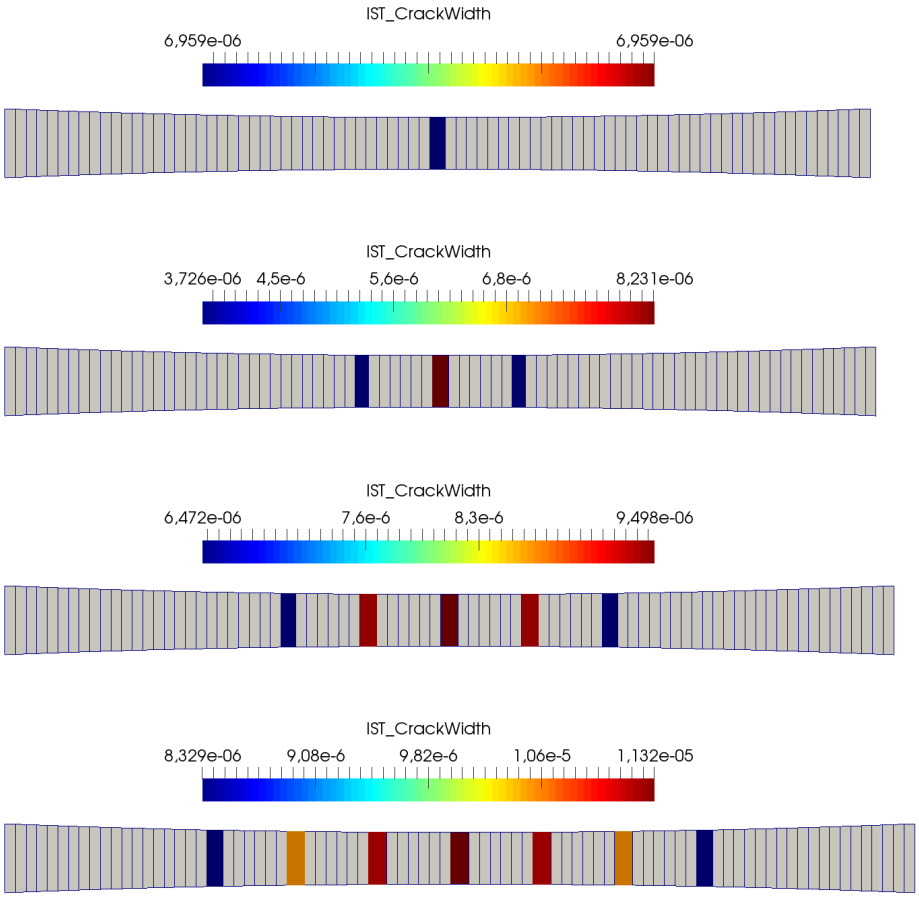

Figure 51: Computed crack widths displayed on a deformed **fine** finite element mesh (the displacements are magnified and the scale is in meters); The distance between cracks as well as the opening is very similar to those from Figure 49.

of the specimen.

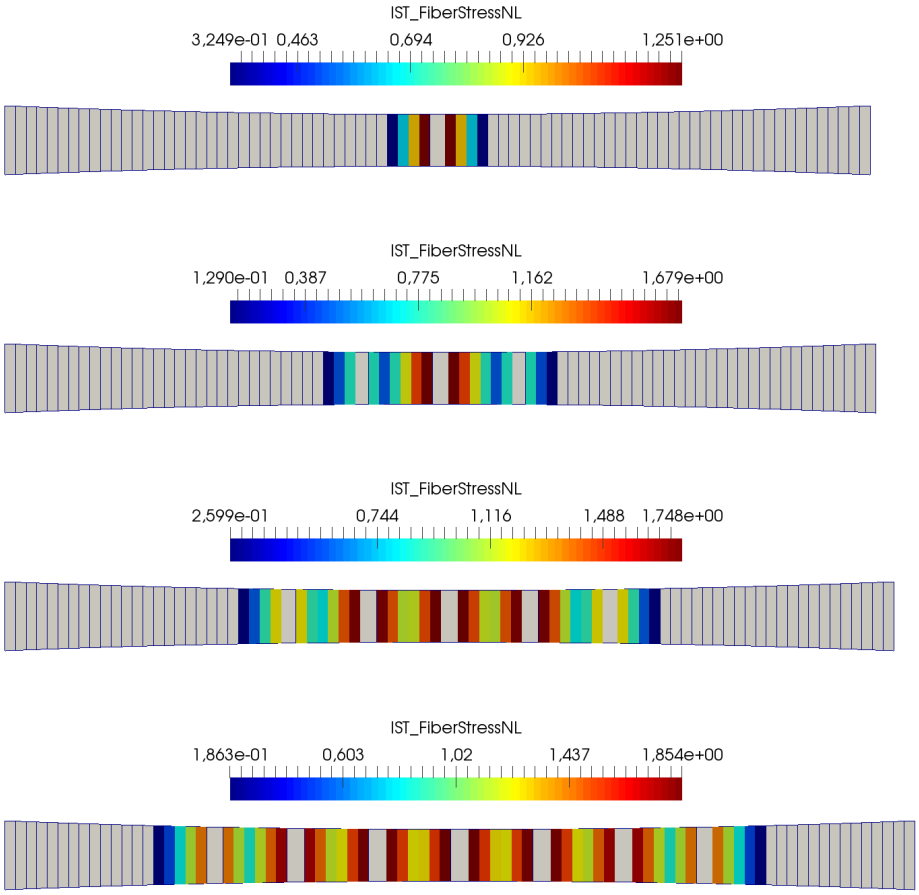

Figure 52: Nonlocal fiber stress in uncracked elements (expressed per unit are of the composite) displayed on a deformed **fine** finite element mesh (the scale is in MPa); the time steps correspond to those from Fig. 50.

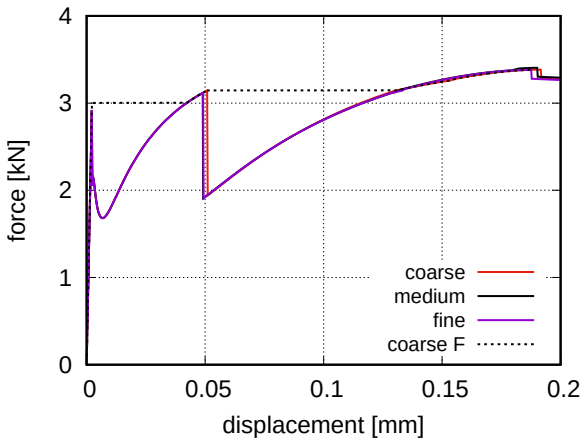

Figure 53: Load-displacement diagram obtained with the **nonlocal** FRCFCM models containing short random fibers; analysis was run under direct displacement and force control and was performed on three different finite element meshes. The figure contains three solid curves which almost impossible to distinguish.

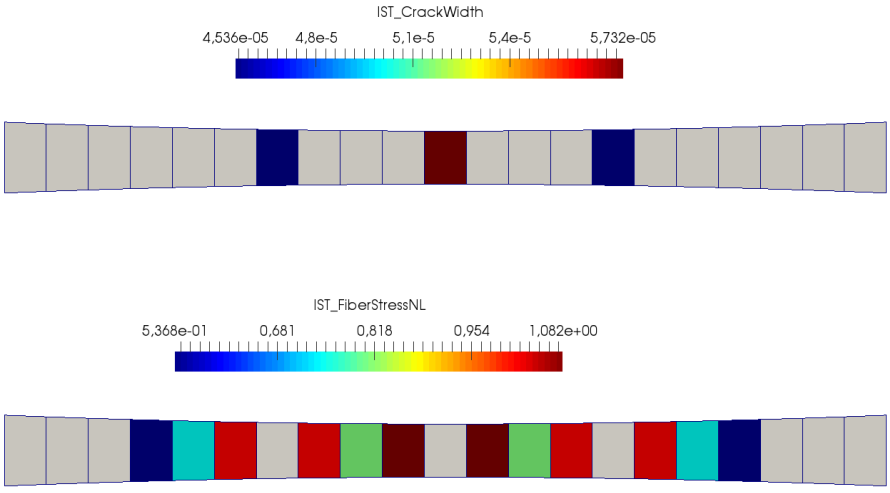

Figure 54: Crack width and nonlocal fiber stress in uncracked elements (expressed per unit are of the composite) computed on a coarse finite element mesh. The results correspond to the loading displacement 0.15 mm.

10 Example: 3-point bending

The nonlocal model for strain hardening cementitious composites is a vital tool not only in specimens which are subjected to almost uniform loading (uniaxial tension, four-point bending), but also when the loading is highly concentrated as demonstrated in this example of eccentric three-point bending. The deformed geometry of the examined specimen is shown in Figure 55. The distance between the middle of the supports is 60 mm and the height is 20 mm. The loading plate is placed at one third of the span. The specimens are labeled according to the number of finite elements per height; Figure 55 shows the coarsest mesh with 10 rows of finite elements. The material uses the definition from the benchmark presented in the previous Section; the fiber class is SRF.

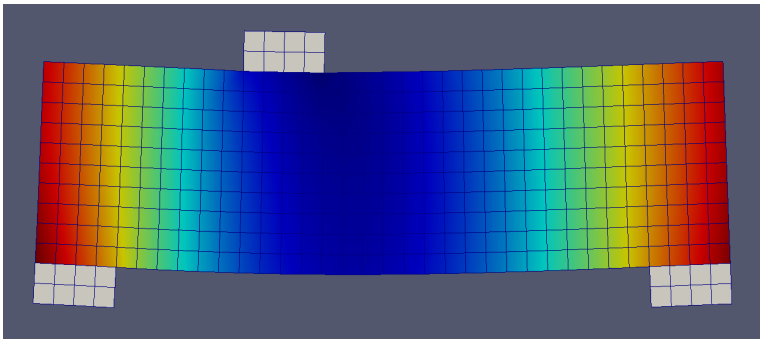

Figure 55: Deformed geometry of the examined beam subjected to three-point bending.

The response of the numerical models with the **local** material law is for the initiation phase shown in Figure 56. The behavior is indeed very ductile, a large number of cracks is formed at the bottom surface under the loading plate. Interestingly, the very first three cracks form similarly – independently whether the local or nonlocal model is used. (The first crack forms under the plate, the second one near the midspan and the third one closer to the left support.) The reason for this is that these cracks are far from each other and therefore do not influence each other by the nonlocal fiber stress. Here, using the local model the cracks are forming in clusters close to the original position of the first three cracks (see Figures 60 and 61), later these clusters merge into a large damaged zone. The collapse occurs when the opening of the crack under the right tip of the loading plate exceeds w^*. The behavior confirms the previous observations: the results are not objective, a finer mesh causes more ductile behavior.

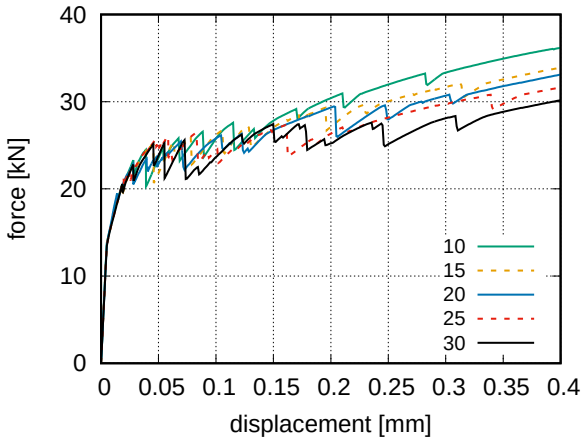

Figure 56: Initiation part of the load-displacement diagram obtained with the **local** FRCFCM model containing short random fibers; analyses were run under direct displacement control and were performed on regular finite element meshes with different nominal element size. The number in the legend corresponds to the number of elements per height.

On contrary to the local model, the **nonlocal extension** provides very consistent results, see Figure 59. The global response is stiffer and the differences between the finest and coarsest model are negligible. However, this is true only for the initiation phase before the global peak. More thorough laws for the mutual crack interaction are necessary to get comparable results also for the postpeak. The crack patterns are shown for the vertical displacement 0.1 and 0.2 mm in Figures 60 and 61. The crack pattern is indeed more realistic than for the local model.

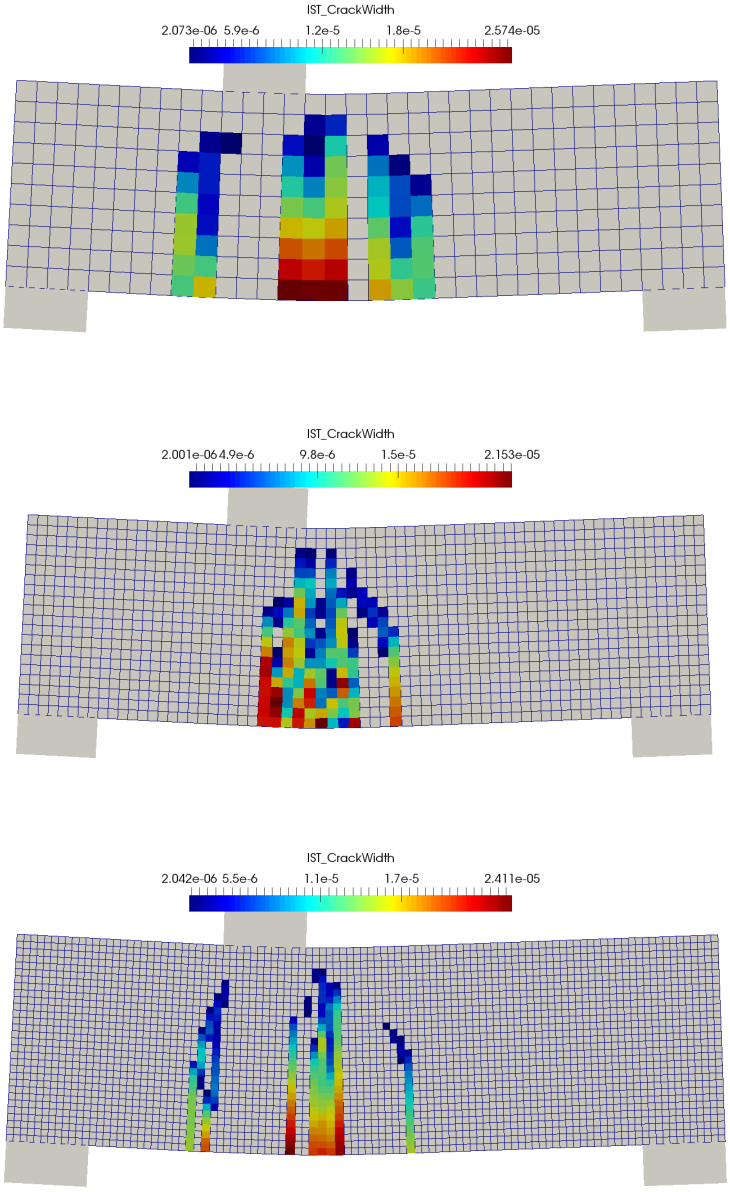

Figure 57: Distribution of crack width computed with the **local** FRCFCM and SRF corresponding to vertical displacement of the loading plate 0.1 mm in models with 10, 20 and 30 rows of finite elements. Elements with crack opening $w < 2\ \mu$m are filtered out.

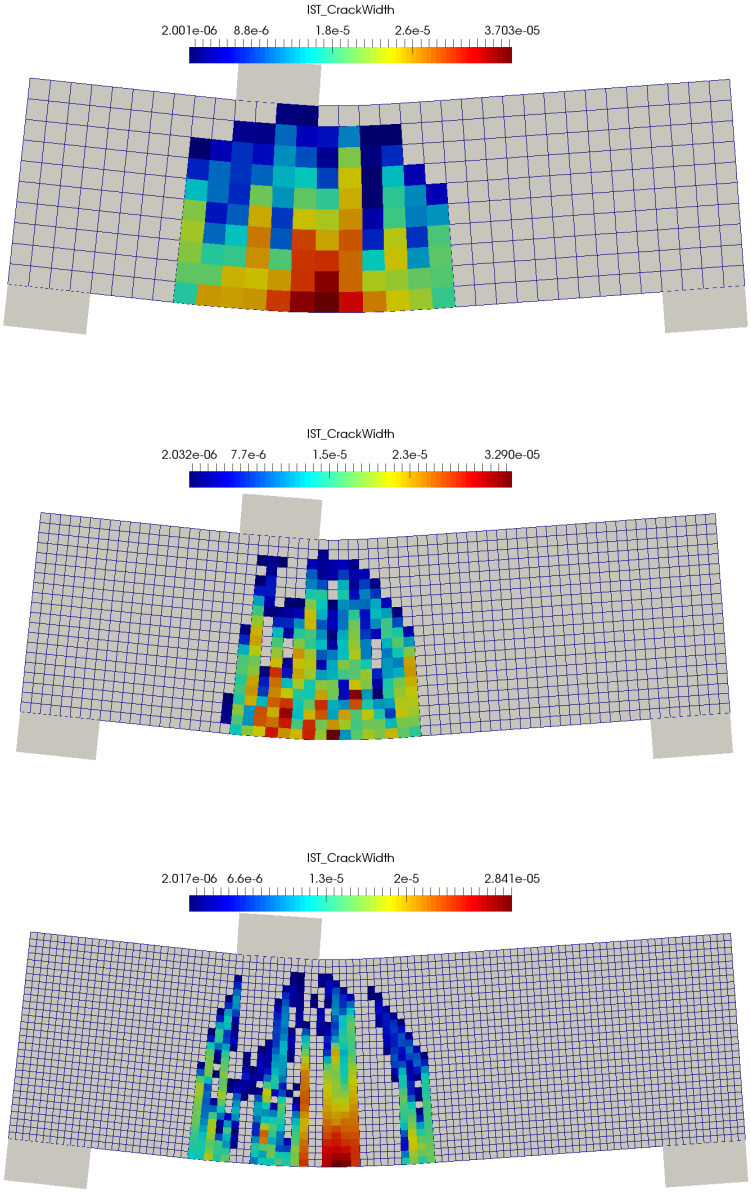

Figure 58: Distribution of crack width computed with the **local** FRCFCM and SRF corresponding to vertical displacement of the loading plate 0.2 mm in models with 10, 20 and 30 rows of finite elements. Elements with crack opening $w < 2\ \mu$m are filtered out.

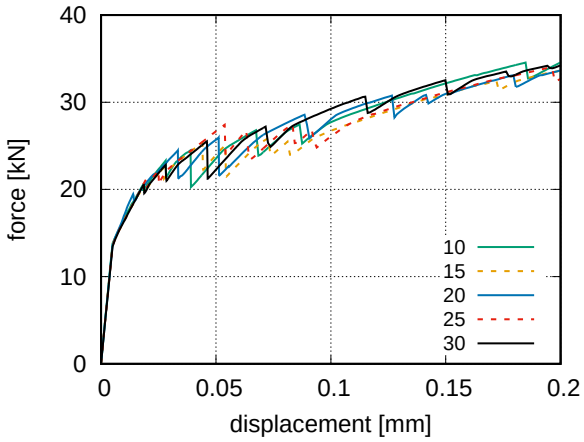

Figure 59: Initiation part of the load-displacement diagram obtained with the **nonlocal** FRCFCM model containing short random fibers; analyses were run under direct displacement control and were performed on regular finite element meshes with different nominal element size. The number in the legend corresponds to the number of elements per height.

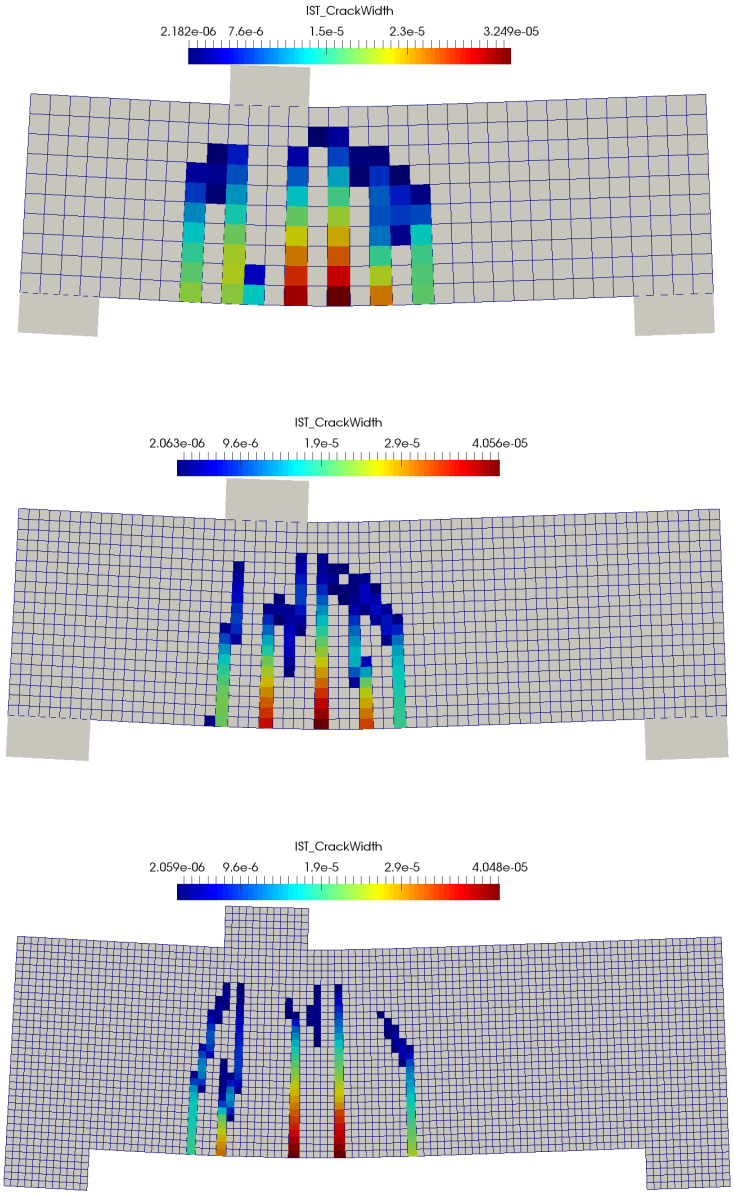

Figure 60: Distribution of crack width computed with the **nonlocal** FRCFCM and SRF corresponding to the vertical displacement of the loading plate 0.1 mm in models with 10, 20 and 30 rows of finite elements. Elements with crack opening $w < 2$ μm are filtered out.

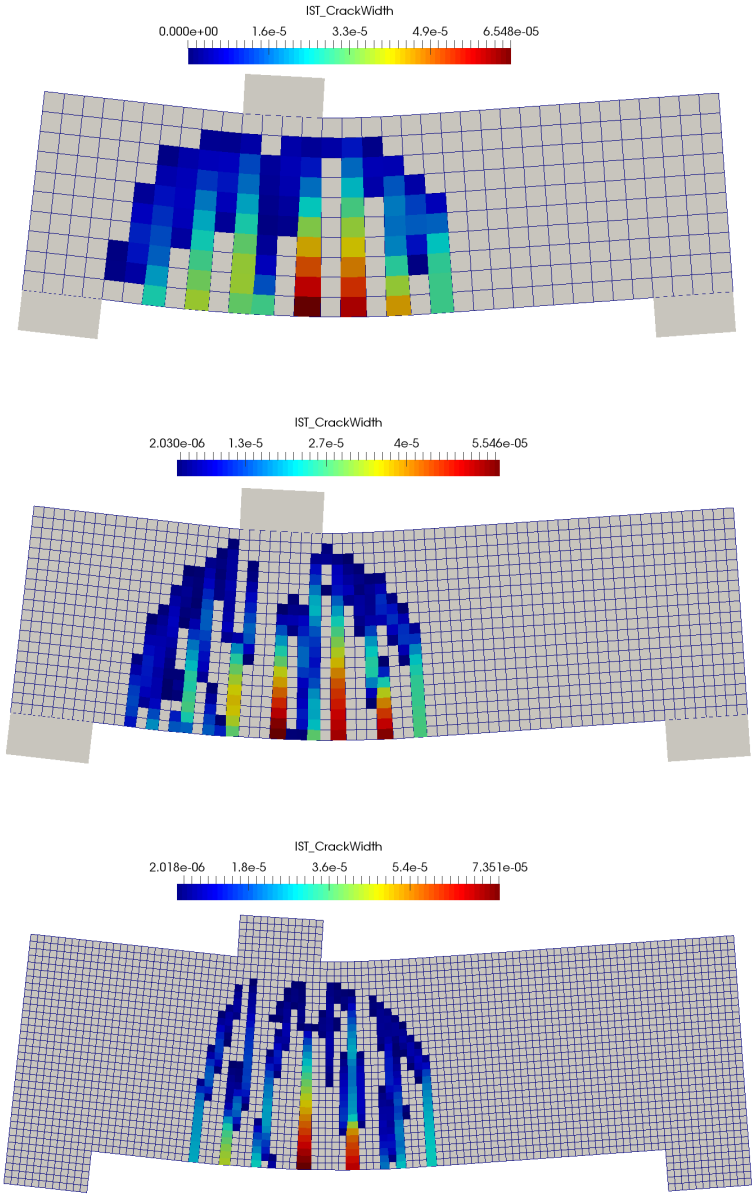

Figure 61: Distribution of crack width computed with the **nonlocal** FRCFCM and SRF corresponding to the vertical displacement of the loading plate 0.2 mm in models with 10, 20 and 30 rows of finite elements. Elements with crack opening $w < 2$ μm are filtered out.

References

[1] J. Aveston and A. Kelly. Theory of multiple fracture of fibrous composites. *Journal of Materials Science*, 8(3):352–362, 1973.

[2] A. Henderson. *ParaView Guide, A Parallel Visualization Appliacation*. Kitware Inc., 2007.

[3] P. Kabele, P. Havlásek, and E. Šmídová. Theoretical manual for the implementation of high performance fibre reinforced cementitious composite material model in ATENA, report VI-2016-01-28, grant number TAČR ta03011564. Technical report, Czech Technical University in Prague, 2016.

[4] C. K. Leung. Design criteria for pseudoductile fiber-reinforced composites. *Journal of Engineering Mechanics*, 122(1):10–18, 1996.

[5] V. C. Li. Postcrack scaling relations for fiber reinforced cementitious composites. *Journal of Materials in Civil Engineering*, 4(1):41–57, 1992.

[6] V. C. Li and C. K. Leung. Steady-state and multiple cracking of short random fiber composites. *Journal of Engineering Mechanics*, 118(11):2246–2264, 1992.

[7] V. C. Li, Y. Wang, and S. Backer. A micromechanical model of tension-softening and bridging toughening of short random fiber reinforced brittle matrix composites. *Journal of the Mechanics and Physics of Solids*, 39(5):607 – 625, 1991.

[8] C. Lu and C. K. Leung. A new model for the cracking process and tensile ductility of strain hardening cementitious composites (shcc). *Cement and Concrete Research*, 79:353 – 365, 2016.

[9] B. Patzák. OOFEM home page. http://www.oofem.org, 2000.

[10] B. Patzák. OOFEM - an object-oriented simulation tool for advanced modeling of materials and structures. *Acta Polytechnica*, 52(6):59–66, 2012.

[11] B. Patzák and Z. Bittnar. Design of object oriented finite element code. *Advances in Engineering Software*, 32(10-11):759–767, 2001.

[12] T. Williams, C. Kelley, and many others. Gnuplot 4.6: an interactive plotting program. http://gnuplot.sourceforge.net/, April 2013.

[13] H.-C. Wu and V. C. Li. Snubbing and bundling effects on multiple crack spacing of discontinuous random fiber-reinforced brittle matrix composites. *Journal of the American Ceramic Society*, 75(12):3487–3489, 1992.

[14] J. Červenka, L. Jendele, and V. Červenka. *ATENA program documentation, part 1, Theory.* Červenka Consulting, 2008.